Solar Viewing Interferometer Prototype

ESTO Final Review

Goddard Space Flight Center
April 2006

Jay Herman	**916**	**Albert Mariano**	**556**
Rick Lyon	**935**	**Nader Abuhassan**	**SSAI**
Severine Tournois	**Sigma**	**Peter Petrone**	**Sigma**
Cheryl Salerno	**544**	**Gary Brown**	**544**

Preliminary Version of 6 April 2006
Final will be delivered in 2 weeks

Observations of the Earth from the Lagrange Points provides unique data that is not available from any other vantage point

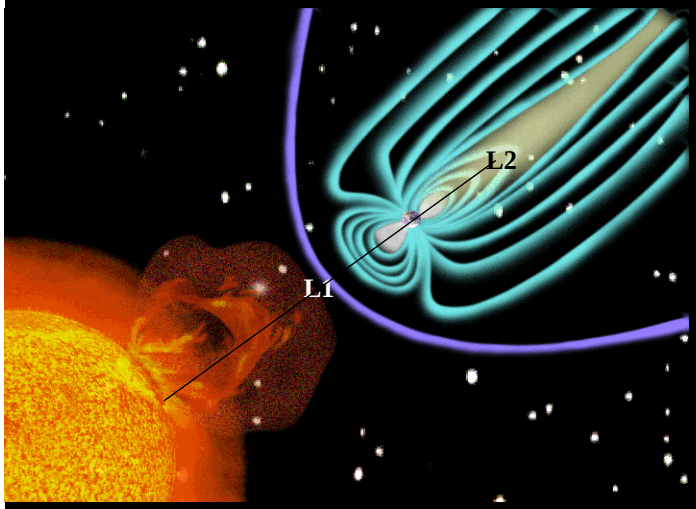

L1 and L2

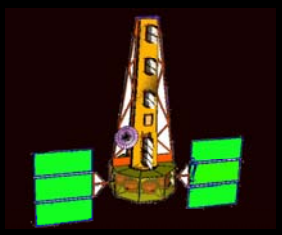

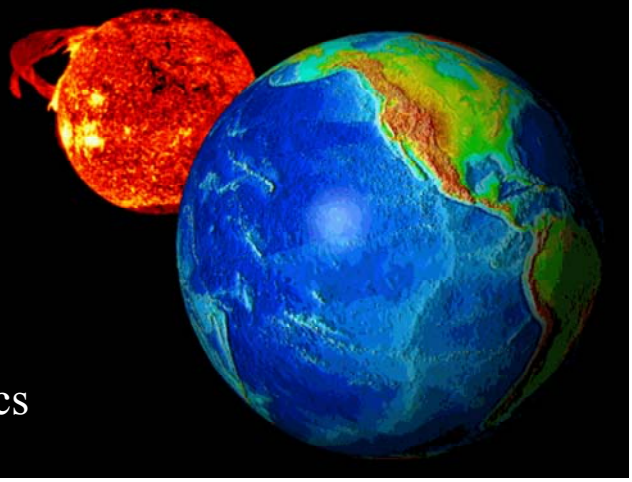

New Technological Development
Synergy with Astronomy Satellites
Greenhouse Gases, Cloud Physics
Aerosols, Ozone, Atmospheric Dynamics

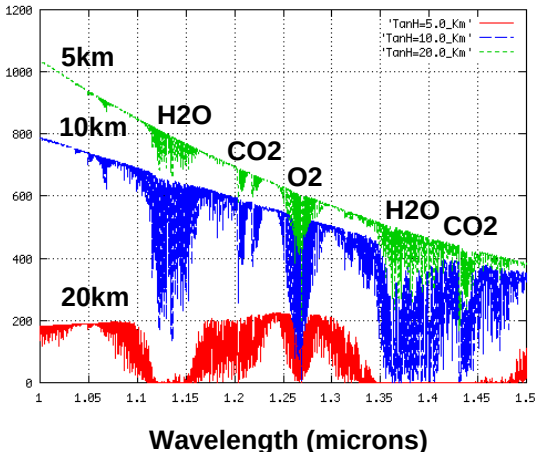

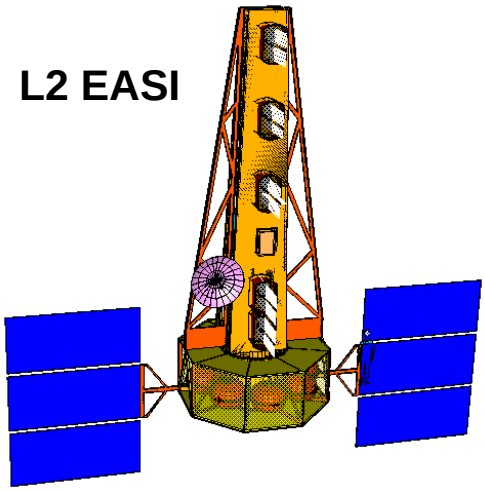

***Earth Atmospheric Solar-Occultation Imager* (EASI) measure Greenhouse Gases (CO2, H2O, CH4, N2O,O2,O3, HCL), precision, completeness of coverage beyond current capabilities.**

- Assess Global Warming, atmos changes, forcings, dynamics, equatorial flow.
- Greenhouse gases (8 km to 30 km), resolution 0.1^0 lat, 2^0 long, 1 km altitude, 1–4 um spectrum
- From L2 –Earth limb occulting, Sun, High solar flux => small collecting area, High spatial resolution (<1 km) => 8 meter 1D boom, w/ 5 – 40 cm telescopes
- ***EASI can be realized with lightweight 1D structurally connected sparse imaging interferometer < 8 m length.***

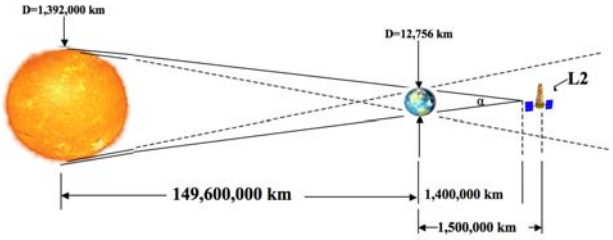

EASI Viewing Geometry

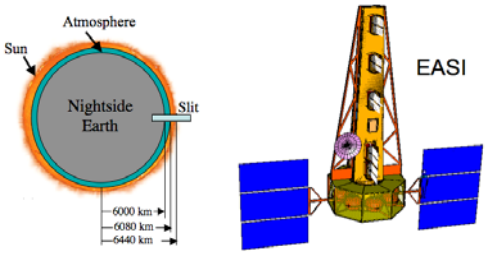

***Solar Viewing Interferometer Prototype* (SVIP): demonstrate needed technologies needed to realize EASI.**

- Demonstrate closed-loop control of optical paths (piston/tip/tip) at 800Hz using extended scenes of the Sun.
- 3 – 10 cm aperture telescopes, 3 delay lines, 3 fast steering mirrors, piston/tip/tilt sensing.
- SVIP Science CO2, O2, H2O.
- Status: fabricated, assembled, final alignment stage.
- Problem: mid-spatial frequencies.

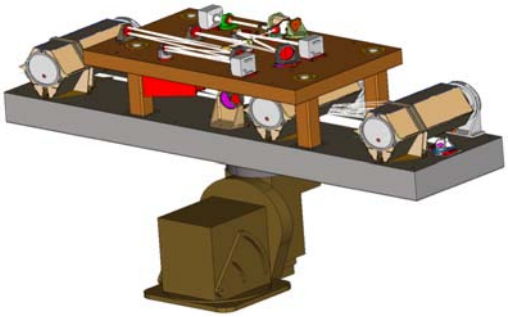

SVIP CAD Model

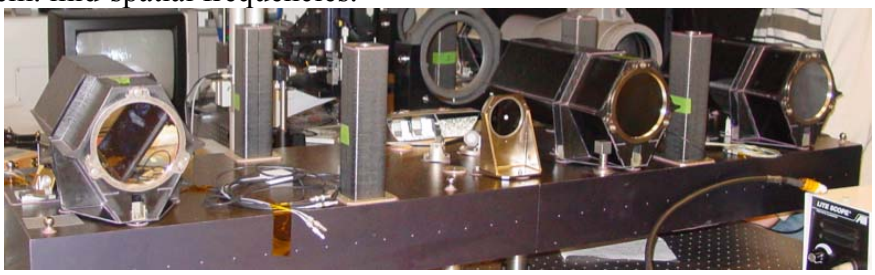

SVIP on Optical Bench

Table of Contents

SVIP Team

Jay Herman (GSFC/613)	Principal Investigator
Rick Lyon (GSFC/606.3)	Co-Investigator
Cheryl Salerno (GSFC/556)	Mechanical Engineer
Peter Petrone (Sigma Space)	Optical Alignment
Nader Abuhassan (SSAI)	DSP and Electronics
Billy Mamakos (Sigma)	Mechanical Layout
Cathy Marx (GSFC/551)	Optical Design

(Probably missing some people here !!!)

1.0 INTRODUCTION

The Solar Viewing Interferometer Prototype (SVIP) IIP project was for development of a 1.2-meter portable interferometer/spectrometer to master the new technology needed for an 8-meter Lagrange-2 (L2) Earth Atmosphere Solar-Occultation Imager (L2-EASI). L2-EASI is an instrument design for an earth-viewing interferometry mission (wavelength: 1 to 4 microns) to measure 2-km resolution altitude profiles of major greenhouse gases (CO_2, O_3, O_2, CH_4, N_2O, H_2O). Figure 1 shows that L2 is the only location where the entire earth can be observed in solar occultation every 24 hours, producing a 3-D mapping of the atmosphere (Altitude-2 km, Latitude-0.5^o, and Longitude-2^o). **Among the results would be the first daily measurements of tropospheric ozone for the entire earth.** Occultation measurements of the Earth's limb from L2 have never been attempted before because of major technical challenges in instrument design. Since useful observations require at least 2 km spatial resolution from an observation point 1.5 million km from Earth, a large 8-meter aperture interferometer is required. Recent optical design studies for L2-EASI have shown that a sparse-aperture 8-meter Fizeau design will easily meet the requirements. Before developing and building such a large instrument, we proposed to develop a small 1.2-meter prototype for ground-based use that will lead to an L2 mission. The goal of the IIP project is to build a working prototype, test the instrument in the laboratory, and possibly under field conditions for measuring greenhouse gases, and to develop data reduction algorithms. The end product will be a scientifically useful instrument that is a proof of concept for a larger space-flight version.

Using solar occultation from Lagrange-2 (L2, a point 1.5 million km behind the earth on the earth-sun line) the global distribution of the major greenhouse gases (CO_2, H_2O, O_2, O_3, CH_4, and N_2O can be observed with ***spectral imaging*** (1 to 4 microns) for the entire earth once per day. The result would be the first daily

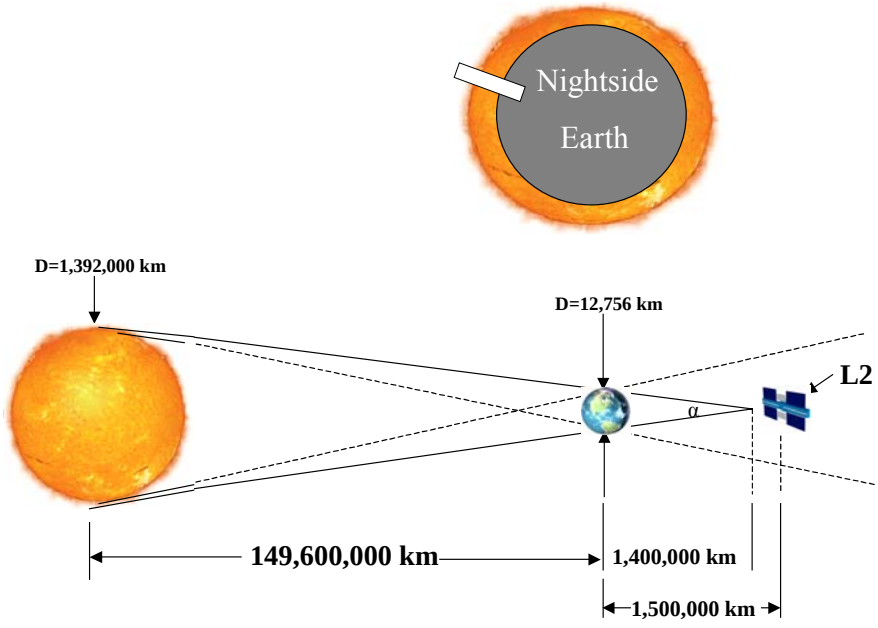

Figure 1 - *Geometry of the view of the earth's atmosphere in solar occultation from L2*. The upper portion is from the viewpoint of L2-EASI looking at the night side earth-sun system from L-2, while the lower portion is a side view from a coordinate system moving with the earth in its orbit about the sun. The rectangle superimposed in the sun and nightside earth is a representation of the interferometer's focal plane. The focal plane is made to rotate about the earth-sun line to view the entire limb once per hour. From the perspective of L2-EASI, the earth rotates so that the entire atmosphere is seen once per day in solar occultation.

3-D global measurements of the earth's atmosphere (altitude-2km from 8 to 30 km, latitude-0.5^o, longitude-2^o). Extensive instrument and spacecraft design studies have shown that it is feasible to construct a Fizeau interferometer capable of observing the earth's atmosphere in solar occultation from L2. While acquiring

observations of the earth's atmosphere, the interferometer would also simultaneously acquire the first high-resolution multi-spectral images of the sun in the 1 to 4 micron wavelength range. Launching a conventional 8-meter circular telescope and spectrometer of this size to look directly at the sun from L2 would be quite daunting and expensive. If nothing else, a suitable circular mirror of this size would require assembly in space to a dimensional precision of fractions of a micron. Dissipation of the solar energy (~1360 watts/m^2) striking the primary mirror and then focused on the secondary mirror may be insurmountable. An alternate method of making the measurement to the required precision and resolution can be accomplished using ***an innovative technology*** mission (Earth Atmosphere Solar-Occultation Imager, L2-EASI), a linear 5-beam sparse-aperture Fizeau interferometer that is 8 meters in length, 1 meter in width, and less than 1.5 meters in depth. The 1.5 meter SVIP is the first sparse-aperture IR Fizeau interferometer for viewing the sun has been built and tested.

The result of building SVIP has been a full check of the design features (e.g., optical delay lines, feedback control systems, tip/tilt mirror mechanisms), which revealed numerous optical and mechanical problems that were solved during the project, and permitted the operating and science algorithms to be developed. The long-term goal of this proposal was to develop the technology to a point suitable for proposing space-flight observations of the earth from L2, and as a stepping-stone in the development of similar astronomical planet-detecting interferometers that are currently being studied.

The L2 space-flight version of the proposed instrument development will establish a unique baseline data set of greenhouse gas distributions for the entire earth from the middle troposphere (8 km) to the middle stratosphere (30 km) and a measure of pressure vs. altitude, all at 2 km altitude resolution. These trace gases comprise the principal greenhouse gases, and are also unique tracers of atmospheric motion and strat-trop exchange. The baseline and time series developed during the lifetime of the instrument (up to about 5 years) would be the basis from which we would be able ***to predict future changes*** in the earth's atmosphere from anthropogenically driven increases in CO_2, N_2O, and CH_4, (2) observe the annual cycle of CO_2, H_2O, O_2, O_3, CH_4, and N_2O, (3) observe upper-tropospheric pollution from lofted airmasses associated with biomass burning and urban pollution, (4) estimate inter-hemispheric transport using CO_2, CH_4, and N_2O as tracers of atmospheric motion, (5) estimate strat-trop exchange using twice per day observations of CO_2, H_2O, O_3, CH_4, and N_2O, (6) observe stratospheric transport phenomena such as the tropical isolation, tropical tape recorder, and the Antarctic ozone hole. The technology development from SVIP would ***enable new measurements that cannot now be made.***

In order to implement these observations over such a 1-4 micron spectral range with a reasonable instrument design, we estimated the sensitivity of the instrument using a bandwidth of 10 nm sampled at ~1 nm. The studied L2 design, using a InSb detector with high precision and a high signal to noise. This approach is in contrast to using extremely high resolution (0.01 nm) in order to resolve individual band features. The benefit is a much more manageable data rate and the need for only 2 focal planes in the instrument design (1 to 2 microns, and 2 to 4 microns. Starting from 1 micron, there are enough single-species band structures that are relatively clear from the absorption of other species to permit the amounts of H_2O, CO_2, and O_2 to be determined directly. The results can then be used to obtain the amount of CH_4. Once CH_4 and H_2O are known, then O_3 and N_2O can be determined. It should be noted that the results would contain **the first daily measurements of middle and upper tropospheric ozone** for the entire globe.

The prototype design is a 1.2 meter Fizeau interferometer employing 3 collimating telescopes, whose path-length matched beams are combined in a grating spectrometer. The resulting dispersed light is imaged on a rectangular IR detector giving wavelength in one direction and spatial imaging in the other direction.

As will be described in more detail later, the spacing of the telescopes is purposely non-uniform to maximize the number of non-redundant path lengths so that maximum spatial resolution can be obtained from a sparsely filled aperture. In the L2 design, 5 non-uniformly spaced telescopes are used to form 9 non-redundant paths so as to nearly uniformly represent all spatial frequency components for resolving spatial variation at the required resolution (2 km). In the 3-telescope ground-based design, much higher spatial resolution will be obtained because of the nearness of the target (~50 km), however, loss in spatial

frequencies will occur due to fewer baselines.

2.0 SVIP IMPLEMENTATION OVERVIEW

2.1 SOLAR VIEWING INTERFEROMETRY PROTOTYPE (SVIP)

SVIP consists of 3 separate 10 cm aperture Gregorian telescopes mounted on a 1.2 meter boom in a non-redundant configuration (Figure 4). SVIP has been packaged and mounted onto a solar tracking stand (Figure 5) where it can perform atmospheric absorption spectroscopy against the solar disk in the 1.25 – 1.73 micron band, at 10 nm spectral resolution and is capable of resolving H_2O, O_2, CO_2, CH_4 (Figure 3) with an angular resolution of 0.26 arcsecs. SVIP has an adaptive optical control system consisting of piston, tip and tilt correction for each of the 3 optical paths with a sampling frequency of 800 Hz and a correction frequency of 200 Hz (3 dB). The piston, tip, tilt is sensed by a suite of sensors and corrected with delay lines and fast steering mirrors to be discussed below.

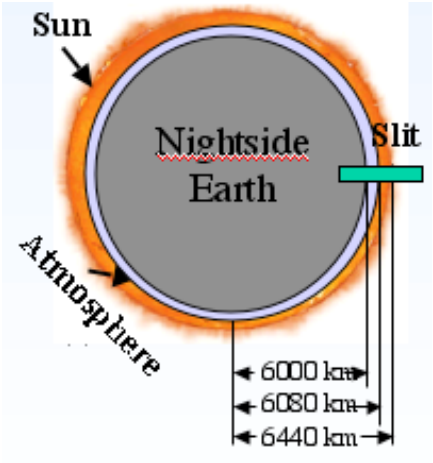

Figure 2 – *Sun-Earth as seen from L2*
Earth occults most of the solar disk.

The primary objectives of SVIP were:

- Demonstrate limited science for EASI; atmospheric spectroscopy occulted against the solar disk.
- Demonstrate scalable wavefront sensing and optical control to EASI
  - Closed-loop Piston/Tip/Tilt control due to atmosphere & boom dynamics
  - aberrations/alignment/FOV/guiding/sensor & actuator noise
  - Assess high bandwidth wavefront control (WFC) strategies
  - Stabilize spectral lines for increased radiometric accuracy
  - Assess Fast Steering Mirror (FSM) and Delay line (DL) technologies
- Develop and validate integrated models for the design and performance prediction of the EASI flight system.
- Identify key technologies needed for EASI and spin-off technology development as needed.

SVIP is formulated in 3 phases. Phase I: A low fidelity laboratory breadboard of a single interferometer channel with one telescope and a single delay line and fast steering mirror. This allowed validation of the wavefront sensing and control electronics and processing, debugging of the DSP architecture and gained experience with the fast steering mirrors and delay lines. Phase II: Medium fidelity laboratory benchtop system consisting of the 3 interferometer channels mounted on the boom, 3 fast steering mirrors and 3 delay lines, a test fixture to generate the input collimated beam, the DSP architecture and the spectrometer. This permitted integrated systems testing and demonstration of closed loop control in a laboratory environment prior to packaging. Phase III: Packaging of SVIP into the instrument box and integration of the instrument with the solar tracking platform and full system testing outside first at GSFC and at a subsequent TBD location.

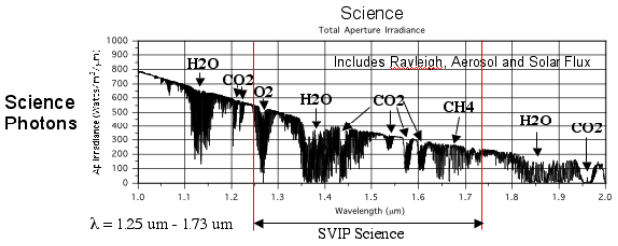

Figure 3 – *SVIP Spectral Passband*

2.2 SVIP DESIGN

Figure 4 shows an optical schematic of SVIP. Light enters the three 10 cm aperture telescopes from the top. The 3 telescopes are elements of the 3 interferometer channels, labeled 1,2 and 3 from left to right

respectively. Telescopes 1 and 2 are spaced by 40 cm on-center and telescopes 2 and 3 are separated by 80 cm on-center, giving a maximum baseline of 120 cm. A reflective aperture mask reflects nearly all but 8% (white light) from entering the telescopes. The reflective aperture mask is essential for the L2-EASI design to keep the solar energy out of the system. Light is incident on the 3 primary mirrors (PM) and subsequent 3 secondary mirrors (SM) of the telescopes. The telescope PM and SM are both concave optics, in an off-axis Gregorian configuration, with an internal focus between the PM and SM and an afocal magnification of 10, thus, the exiting beams are 1 cm in diameter. A Gregorian configuration is used since it has a real pupil image on the subsequent fast steering mirrors (FSM). The 3 telescopes are mounted a boom structure. The field of view of the system is +/- 15 arcseconds in both along-boom and the cross-boom directions. Following the telescopes are the FSMs, 3 in all, 1 per channel, each is a flat mirror. The FSMs comprise the limiting stop of the system and thus define the entrance pupils for each of the 3 interferometer channels. The FSMs move in tip/tilt to counter atmospheric and boom induced tip/tilt. Following each of the FSMs are 3 delay lines. Each delay line (DL) is a retroreflector consisting of 2 mirrors mounted at 90 degrees to each other. The DL's translate in the along beam direction to compensate for path length errors induced by atmospheric turbulence and boom dynamics. The requirements for the FSMs and DL's will be discussed in below. After the 3 DL's are 3 relay flats at 45° to the beams. These flats relay the beams to a single concave primary mirror of the beam combiner (PMBC). At the PMBC the 3 beams are each 1 cm in diameter and are separated by 4 cm on-center for beams 1 and 2 and 8 cm on-center for beams 2 and 3. The PMBC is rectangular in shape. The secondary mirror of the beam combiner (SMBC) is a concave mirror that subsequently focuses the 3 beams to a common focus at the entrance slit of the spectrometer (not shown). The spectrometer design is discussed in below. Prior to the spectrometer slit but after the SMBC, the light is split into multiple optical paths via a series of beamsplitters. Light from λ = 1.25 – 1.73 microns continues through the beamsplitters to the science spectrometer. Light from λ = 0.4 – 1.0 microns (Figure 6) is relayed to the tip/tilt sensors and to the differential piston sensors. There are 3 tip/tilt sensors, one per interferometer channel (beam) and 2 differential piston sensors one for beam pairs 1 and 2 and one for beam pairs 2 and 3. These are not shown in Figure 4 but are developed in more detail in later sections. The tip/tilt sensors and differential piston sensors operate at 800 Hz, i.e. the frame rate of their CCD array detectors is 800 frames per second. Data from the CCD array detectors is processed by a DSP computer (Figure 7) and fedback to the fast steering mirrors and delay lines at 200 Hz. This combination of sensors, processor, feedback, controllers and FSMs and DL's serves as the wavefront sensing and control system and serves to correct for atmospheric induced piston, tip and tilt and for the dynamics of the boom and mounting structures.

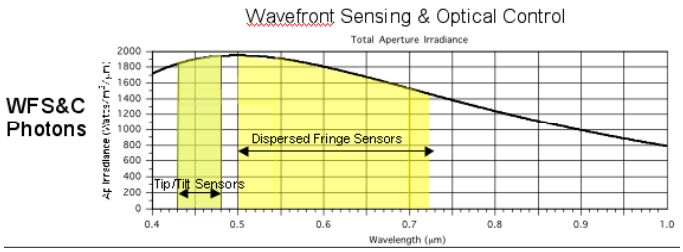

Figure 6 – *Spectral passbands of Piston and Tip/Tilt Sensors*

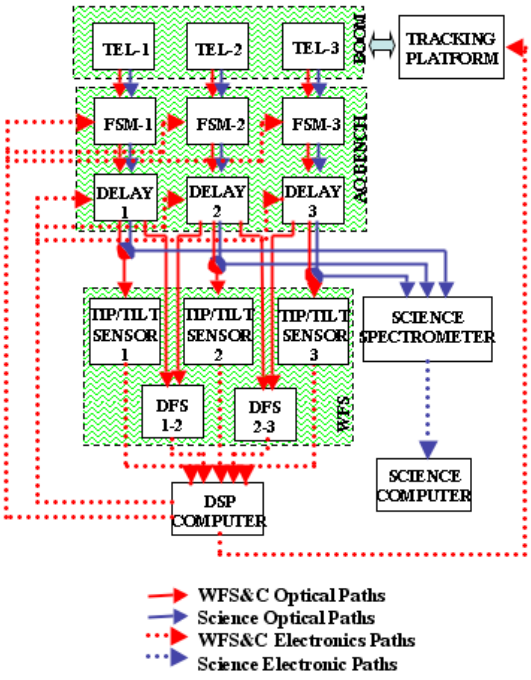

Figure 7 – *SVIP Control System*

The top-level block diagram for the SVIP wavefront sensing and optical control (WFS&C) system is shown in Figure 7. The WFS&C optical paths are shown in solid red and the science optical paths are shown in

solid blue. The WFS&C data and electronics paths are shown in dotted red and the science data and electronics paths are shown in dotted blue. Data from the 3 detectors in the 3 tip/tilt sensors are fed back to the 3 FSM mirrors and the solar tracking platform to maintain relative pointing between the telescopes and global pointing of the entire structure. Data from the 2 differential piston sensors are fedback to the 3 delay lines to maintain equal path lengths between the 3 beams.

2.3 ERROR BUDGETING

A simplified top-level *closed-loop* error budget is described; the full error budget for the system would occupy too much space in this manuscript, but is available in spreadsheet form. The closed-loop error budget assumes the wavefront sensing and optical control system is operational and hence piston, tip/tilt and global pointing are compensated.

The total wavefront variance, in units of waves at 1.0 micron, during closed-loop control is given by:

$$\sigma^2_{WFE} = \sigma^2_{ideal} + \sigma^2_{\Delta t} + \sigma^2_{optics} + \sigma^2_{Tip/tilt\ sensors} + \sigma^2_{Piston\ sensors} + \sigma^2_{FSM} + \sigma^2_{DL} + \sigma^2_{Drift} \quad (1)$$

where σ_{ideal} is the residual turbulence with perfect correction of piston, tip and tilt at infinite bandwidth and is due to spatial modes other than piston, tip and tilt. The total uncorrected turbulence across the 3 apertures is given by [1]:

$$\sigma^2_{uncomp} = 0.0258\left(\frac{D}{r_0}\right)^{\frac{5}{3}} + 0.174\left(\frac{B_{12}}{r_0}\right)^{\frac{5}{3}} + 0.174\left(\frac{B_{23}}{r_0}\right)^{\frac{5}{3}} \quad (2)$$

where D is the diameter of a single aperture (10 cm) and B_{12} and B_{23} are the baselines between apertures 1 and 2 (40 cm) and apertures 2 and 3 (80 cm) respectively; r_0 is the Fried parameter and represents the atmospheric spatial correlation length, assuming a reasonably quiescent night yielding an $r_0 = 10$ cm gives $\sigma_{uncomp} = 2.711\lambda$ where λ is at a wavelength of 1 micron. This represents an average worst-case scenario. The ideal case is given by $\sigma^2_{ideal} = 0.0034\left(\frac{D}{r_0}\right)^{\frac{5}{3}}$ or $\sigma_{ideal} = 0.058\lambda$ thus the extremes with no wavefront correction and with ideal wavefront correction are bounded as ~0.06 waves to ~2.7 waves. Any wavefront control scheme will necessarily be less than ideal, thus the true value will fall between these bounds and contains errors due to the temporal delays (latency and control bandwidth), optics, tip/tilt sensors, piston sensors, fast steering mirrors, delay lines and thermal and mechanical drift. The error due to temporal delays is given by $\sigma^2_{\Delta t} = 0.719\left(f_G / f_B\right)^{\frac{5}{3}}$ where f_G (~60 Hz) and f_B (800 Hz) are the atmospheric correlation time and control bandwidth respectively. Encapsulating all this into an error budget formalism (Figure 8) shows that we expect to obtain and overall wavefront error of 0.1683 waves or ~λ/6 at λ = 1 micron or ~λ/7.5 at our science wavelength of 1.25 microns.

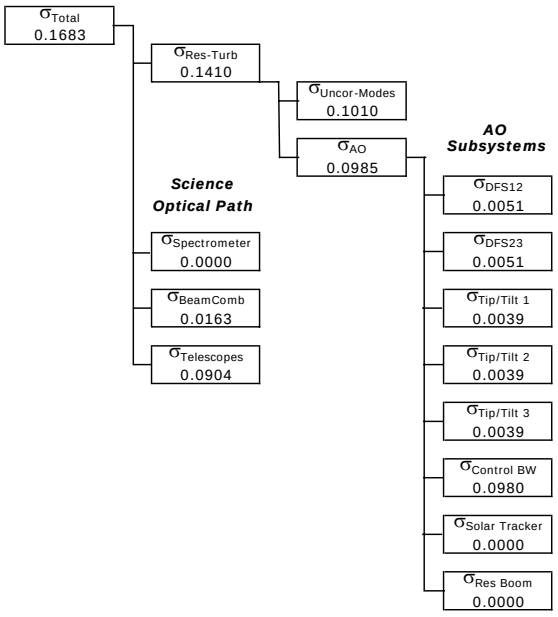

Figure 8 – *SVIP Top-Level Error Budget*

3.0 WAVEFRONT SENSING AND OPTICAL CONTROL

The wavefront sensing and optical control sub-system consists of 3 tip/tilt sensors, 2 differential piston sensors, an active optical bench with 3 fast steering mirrors (FSM) and 3 delay lines, the DSP processing computer and the solar tracking platform.

3.1 TIP/TILT SENSORS

There are 3 tip/tilt sensors, one per telescope channel; an optical layout of a single sensor is shown if Figure 9. Each tip/tilt sensor is optically fed by a 1 cm diameter beam from one of three partially reflecting beam splitters after the beam combiner secondary mirror. These 3 beamsplitters are after the 4 beamsplitters for the differential piston sensor. Each beam is spectrally filtered to 0.455 microns with a full-width-half-max (FWHM) bandpass of 0.050 microns using a bandpass filter. In this band solar granulation has approximately 10% contrast and high contrast sunspots are also visible with enough contrast to drive the sensors (Figure 5). In each tip/tilt sensor a single focusing lens brings the beam to focus on a detector array. There are 3 lenses and 3 detectors arrays, 1 per telescope channel.

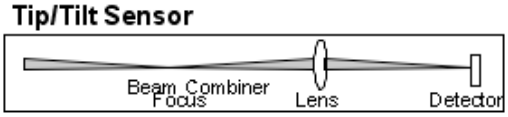

Figure 9 – *SVIP Tip/Tilt Sensor*

The 3 arrays are readout and processed through the matched filtering algorithm by the DSP computer. The outputs are the 3 wavefront tips and 3 wavefront tilts, 6 numbers. These are fed back to the 3 fast steering mirrors and solar tracking platform. The width of the focal plane array is driven by the angle-of-arrival fluctuations and the modal deflections of the boom. The angle of arrival fluctuations are drive the detector width to $W_\theta = 5.308\text{x}10^5 (D/r_0)^{5/6}(\lambda/D)$ arcseconds; for $D = r_0 = 10$ cm and $\lambda = 0.455\ \mu m$, or $W_\theta = 2.415$ arcseconds in object space. The requirement for a 1 sigma deflection of the boom is 25 microns over 1.2 meters, giving 4.297 arcseconds of deflection in object space. RSS'ing the angle of arrival variation with the boom deflection gives $W_\theta = \sqrt{(2.415)^2 + (4.297)^2} = 4.929$ arcseconds in object space. The requirement of σ = 0.08 arcseconds over 3 channels gives $\sigma = (1/\sqrt{3})0.08 = 0.046$ arcseconds/channel or a desired sampling of 0.023 arcseconds/pixel, i.e. the plate scale. This gives a detector size of 4.929/0.023=214 pixels, or rounding up to next power of 2 gives a tip/tilt detector array size of 256 x 256.

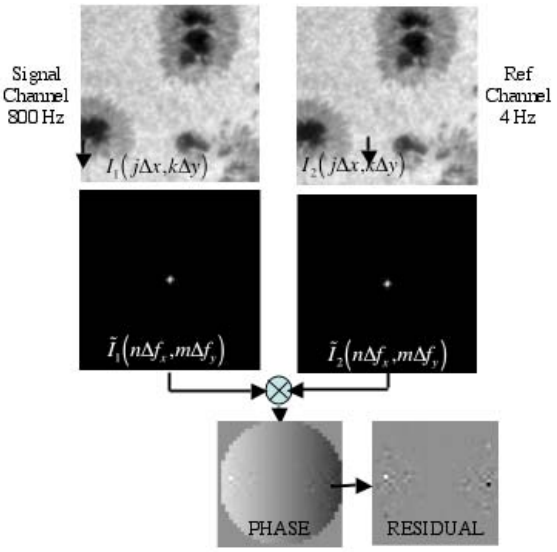

Figure 10 – *Phase Correlation Algorithm*

A 256 x 256 detector operating at 800 frames/sec requires a single port detector to operate at ~52 Mhz. Solar granulation of 10% with a 12 bit detector gives all the signal in the top 410 ADU's. A full well of 100,000 electrons at 12 bits gives ~24 electrons/ADU with a theoretical peak SNR of 316.

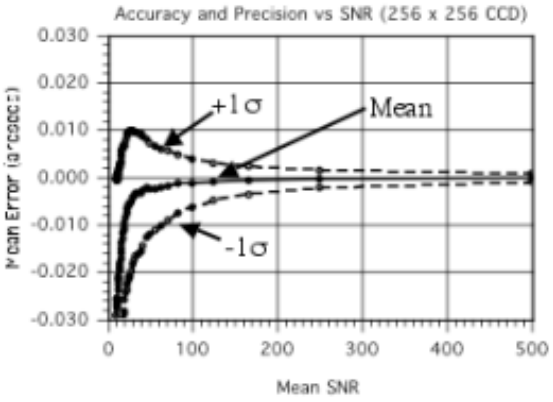

Figure 11 – *Accuracy and Precision of Tip/Tilt Sensor*

Phase Correlation Algorithm

The tip/tilt sensors utilize a phase correlation algorithm that fits the phase of the cross-correlation between a signal channel and the reference channel. The reference channel is channel 2, i.e. the middle telescope image, it is buffered at 4 Hz (i.e. every 0.25 seconds) and cross-correlated against channels 1 and 3 at 800 frames per second and against channel 2 at 800 frames per second. Thus the reference channel is allowed a slow drift which is fed back to the solar tracking station to stay on target. The phase correlation algorithm is computationally fast on the DSP architecture and a description of the algorithm follows.

Let $I_1(j\Delta x, k\Delta y)$ and $I_2(j\Delta x, k\Delta y)$ represent the discretely sampled signal and reference images respectively (top row of Figure 10) and let $\tilde{I}_1(n\Delta f_x, m\Delta f_y)$ and $\tilde{I}_2(n\Delta f_x, m\Delta f_y)$ represent their 2D fast Fourier transforms (FFT) (middle row of Figure 10). Then calculate the complex phasor given by:

$$R_{nm} = \frac{\tilde{I}_1(n\Delta f_x, m\Delta f_y)\tilde{I}_2^*(n\Delta f_x, m\Delta f_y)}{\left|\tilde{I}_1(n\Delta f_x, m\Delta f_y)\tilde{I}_2^*(n\Delta f_x, m\Delta f_y)\right|} = e^{i\phi(n\Delta f_x, m\Delta f_y)} \tag{3}$$

and fit the phase to $\phi_{nm} = An\Delta f_x + Bm\Delta f_y + C$, (bottom left Figure 10) the resulting coefficients A and B are proportional to the tip and tilt. In practice, there a few more steps due to extracting the phase of the phasor due to the phase being recovered modulo 2π, however the algorithm only requires 840 MFLOPS per channel and has already been successfully implemented on the architecture. Figure 11 shows the accuracy and precision versus mean image SNR calculated via a Monte-Carlo simulation of the process; for SNR > 12 the mean error (accuracy) is better than 0.023 arcseconds with a precision of 0.023 arcseconds.

3.2 DIFFERENTIAL PISTON SENSORS

The differential piston sensors are based on dispersed fringe sensing. There are two dispersed fringe sensors, one that mixes channels 1 and 2 and the 2nd that mixes channels 2 and 3. Each of the two differential piston sensors contains a collimating lens that re-images the exit pupil onto a diffraction grating, and a focusing lens that focuses the dispersed beam onto the detector (see Figure 12). In practice we have already adapted the design using a curved grating to remove the focusing element. Beams, 1, 2 and 3, from the beam combiner secondary mirror, have dichroic beamsplitters, which split off the some of the photons 0.4 – 1.0 microns for the differential piston sensors. Beams 1 and 3 both have a single beam splitter with intensity reflectivities of 33%. Beam 2 has 2 beamsplitters, the first of which splits off 33% of the photons short of 1.0 microns and the second splits of 50% of the remaining 66% photons. Thus, both differential piston sensors have equal energy in each channel. Following the beam splitters are 2 collimating lens, one for each of the differential piston sensors (DPS). DPS12 mixes beams 1 and 2, and DPS23 mixes beams 2 and 3. Within each of the DPS's is a diffraction grating, focusing lens and a CCD array.

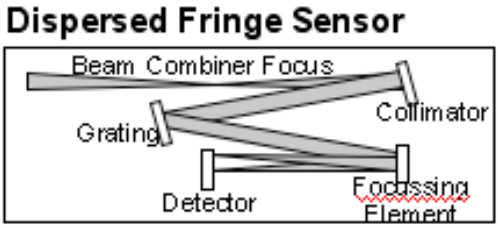

Figure 12– *Differential Piston Sensors*

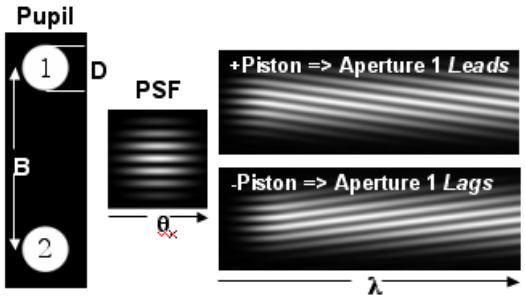

Figure 13 – Simulated Outputs of DFS

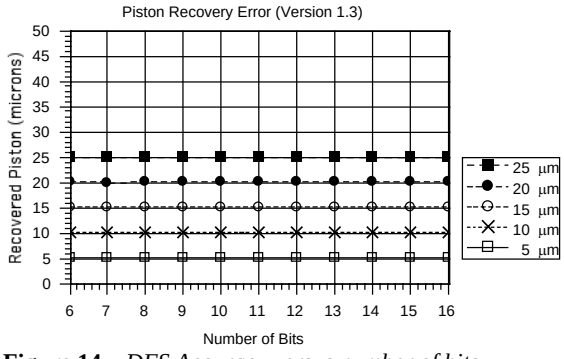

Figure 14 – *DFS Accuracy versus number of bits*

Figure 13 shows the output (simulated) from a DFS. The rightside shows the dispersed "barbershop pole" patterns which contain the piston information encoded within the spacing between successive maxima. With no piston the lines in the dispersing direction would be straight. The amount of spiral and the direction give the piston. Even with other aberrations and tip/tilt the DFS is very robust in piston sensing over a large range.

A number of different algorithms were tried for extracting the piston from the fringe pattern, however, the one we settled on, due to numerical efficiency and hence bandwidth, is a clustered least squares which fits the data to a function data = Ax^2+Bx+C within a sliding window and calculates the maximum within the window as –B/2A, C is not calculated since not needed. As a window slides multiple realizations of the same maxima are found giving a robust estimator. Fits across multiple scan lines identify which aperture is leading or lagging the other in piston. The algorithm is numerically efficient (640 MFLOPS aggregate for both channels) and results in an accuracy of better than 0.1 microns of piston difference (Figure 14).

3.3 CONTROL MATRIX

The 3 tip/tilt sensors and the 2 dispersed fringe sensors give 8 measurements as a function of time; shown as the vector on the right side of equation (4). The first 2 components represent the differential piston terms between channels 1 and 2 and the next 3 terms the tip of telescopes of 1, 2, and 3 respectively, and the last 3 terms the tilt of telescopes of 1,2 and 3 respectively. The left hand side of equation (1) represents the control degrees of freedom (DOF), 11 DOF in all. The first 3 are the pistons of the delay lines 1, 2 and 3 respectively. The next 3 are the tips of each of the 3 fast steering mirrors (FSM) at the locations of the FSMs; the following 3 are the tilts of the 3 FSMs at the locations of the FSMs. The last 2 are tip and tilts used to drive the tracking station. The number of control degrees of freedom is greater than the number of measurements. This is due to requiring the mean piston, tip and tilt be maintained at zero at 800 Hz and fed back to the DLs and FSMs . This insures that the actuators do not use up their range and is also the reason why there are 3 delay lines and fast steering mirrors. The mean tip/tilt is fed back at 4 Hz to the solar tracking platform to maintain overall SVIP pointing. The matrix which maps measurements to control DOFs is shown in equation 1 and contains the constraints of mean piston, tip/tilt being maintained at zero. This matrix insures that the piston remains mean zero as a function insuring against a bias drift which uses up the dynamic range of the delay lines. Similarly, it insures that the mean tip and tilts as a function of time remains mean zero preventing a pointing error that would be corrected by the FSM instead of the tracking station.

$$\begin{bmatrix} P_1 \\ P_2 \\ P_3 \\ \theta_{x1} \\ \theta_{x2} \\ \theta_{x3} \\ \theta_{y1} \\ \theta_{y2} \\ \theta_{y3} \\ \theta_{x123} \\ \theta_{y123} \end{bmatrix} = \begin{bmatrix} -2/3 & -1/3 & 0 & 0 & 0 & 0 & 0 & 0 \\ 1/3 & -1/3 & 0 & 0 & 0 & 0 & 0 & 0 \\ 1/3 & 2/3 & 0 & 0 & 0 & 0 & 0 & 0 \\ 0 & 0 & -2m_a/3 & m_a/3 & m_a/3 & 0 & 0 & 0 \\ 0 & 0 & m_a/3 & -2m_a/3 & m_a/3 & 0 & 0 & 0 \\ 0 & 0 & m_a/3 & m_a/3 & -2m_a/3 & 0 & 0 & 0 \\ 0 & 0 & 0 & 0 & 0 & -2m_a/3 & m_a/3 & m_a/3 \\ 0 & 0 & 0 & 0 & 0 & m_a/3 & -2m_a/3 & m_a/3 \\ 0 & 0 & 0 & 0 & 0 & m_a/3 & m_a/3 & -2m_a/3 \\ 0 & 0 & -1/3 & -1/3 & -1/3 & 0 & 0 & 0 \\ 0 & 0 & 0 & 0 & 0 & -1/3 & -1/3 & -1/3 \end{bmatrix} \begin{bmatrix} \Delta P_{12} \\ \Delta P_{23} \\ \Delta\theta_{x1} \\ \Delta\theta_{x2} \\ \Delta\theta_{x3} \\ \Delta\theta_{y1} \\ \Delta\theta_{y2} \\ \Delta\theta_{y3} \end{bmatrix} \tag{4}$$

4.0 OPTICAL SYSTEM

4.1 OPTICAL DESIGN OVERVIEW

The table below is a summary of the F#, Airy disk size and depth of focus

SVIP F# SUMMARY

Depth of focus	+/- 2 lambda F#^2
Airy disk diam (84% energy)	2.44 lambda F#

<u>At telescope field stop:</u>		
PM focal length	250	mm
Beam size at PM	100	mm
F# (FL/beam size)	2.5	
<u>At BC focus:</u>		
BC EFL	2000	mm
Beam size at BC PM	10	mm
F# (EFL/size beam)	200	
<u>At tip/tilt image plane (at camera):</u>		
distance from lenslet to image plane	57	mm
beam size at lenslet	0.6	mm
F#	95	

At telescope field stop (internal focus)		**At BC focus**		**At tip/tilt detector**		
wave (microns)	Depth focus (+/-) (microns)	wave (microns)	Depth focus (+/-) (microns)	wave (microns)	Depth focus (+/-) (microns)	
0.43	5.4	0.43	34400.0	0.43	7762	
0.45	5.6	0.45	36000.0	0.45	8123	
0.48	6.0	0.48	38400.0	0.48	8664	
0.5	6.3	0.5	40000.0			
0.613	7.7	0.613	49040.0			
0.633	7.9	0.633	50640.0			
0.727	9.1	0.727	58160.0			
1	12.5	1	80000.0			
1.25	15.6	1.25	100000.0			
1.4	17.5	1.4	112000.0			
1.63	20.4	1.63	130400.0			
wave (microns)	Airy disk diam (microns)	wave (microns)	Airy disk diam (microns)	wave (microns)	Airy disk diam (microns)	(pixels)
430	2.6	0.43	210	430	99.7	8.3
450	2.7	0.45	220	450	104.3	8.7

480	2.9	0.48	234	480	111.3	9.3
500	3.1	0.5	244			
613	3.7	0.613	299			
633	3.9	0.633	309			
727	4.4	0.727	355			
1000	6.1	1	488			
1250	7.6	1.25	610			
1400	8.5	1.4	683			
1630	9.9	1.63	795			

4.2 BEAMSPLITTERS

After the SMBC, the light is split into multiple optical paths via a series of beamplitters. Fig.1 shows a schematic of the required reflected and transmitted wavelengths. Light with wavelengths larger than 1250 nm will be relayed to the spectrometer after reflection off BS1. Light with wavelengths smaller than 727 nm will continue through BS1. BS2 reflects wavelengths shorter than 480 nm and transmits wavelengths larger than 500 nm. BS3 is a 50/50 beamplitter. It does not separate wavelengths.

BS1 was difficult to find on the commercial market. It is a custom fused silica plate. BS2 is an inexpensive off-the-shelf fused silica plate designed for Raman Spectroscopy. BS3 is a custom BK7 plate with a standard broadband 50/50 coating. The bandpass filter is an inexpensive off-the-shelf BK7 60 nm band filter centered at 447 nm.

Details about R% and T% for the beamsplitters are presented in Appendix ???.

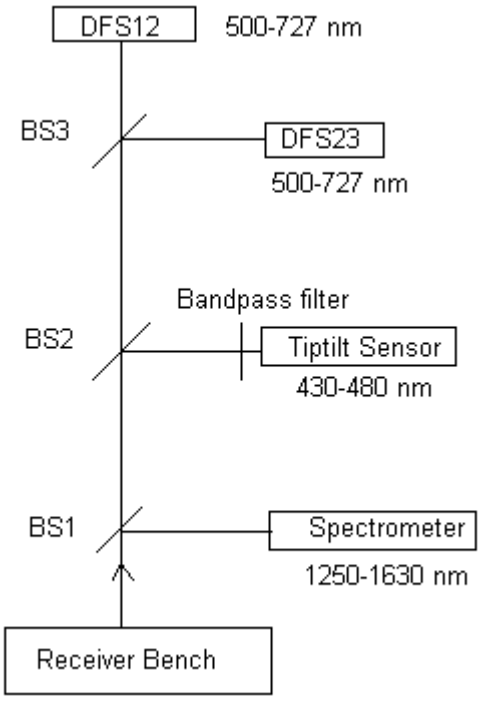

Fig.1 Schematic of the required reflected and transmitted wavelengths

4.3 TIP/TILT SENSOR

The three beams coming from the three telescopes come together in focus (they overlap). A field mask is placed at the focus in order to limit the field to a square 60x60". There are three tip/tilt sensors, one per telescope channel. In each tip/tilt sensor a single focusing lens brings the beam to focus on a detector array (Fig.2).

A relay lens (sometimes called "field lens" in the reports) is placed just after the field mask. The relay lens has no effect of the center beam (on-axis field). It has an effect on the off-axis beams. Its role is to "bend" the series of three beams so that the beams issued from all fields overlap and thus relay the pupil (Fig.3).

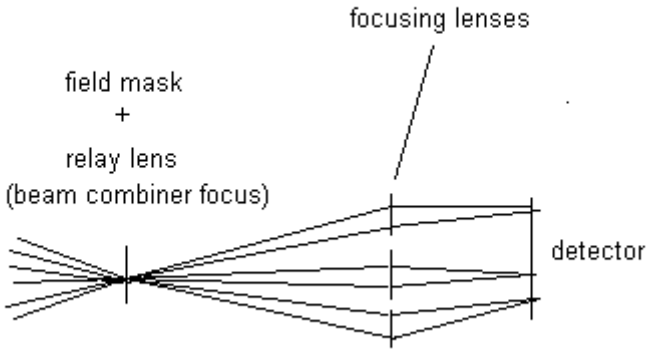

Fig.2 Schematic of the three tip/tilt sensors (only one field shown)

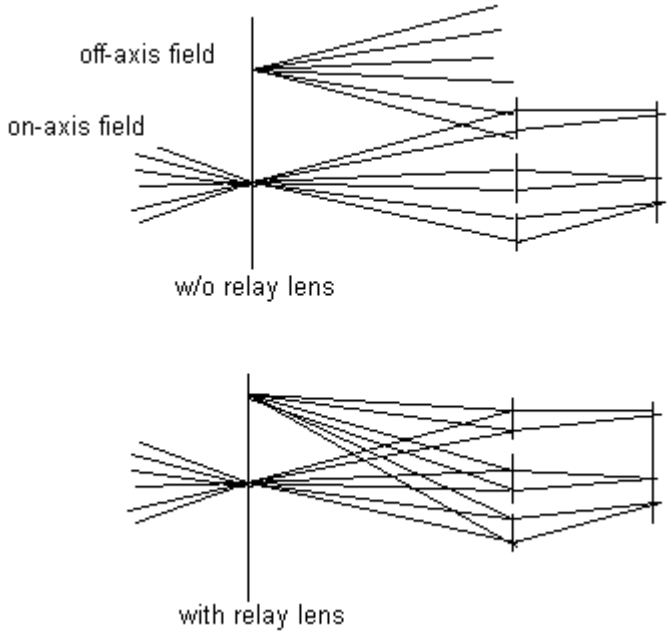

Fig.3 Schematic of the tip/tilt sensors showing role of the relay lens (2 fields shown)

In an early design the beams were focused by 3 separate lenses on 3 separate detectors. But in July 2004, an analysis showed that this configuration had problems of instability.
(show instability analysis here or in appendix)

The 3 lenses would have to be extremely stable in order to avoid unwanted relative changes between the 3 images. This extreme stability could not have been achieved in practice. It became necessary to modify the design. We came up with the idea of using a monolithic microlens array. The 3 focusing lenses would be made in one single substrate. This would eliminate the concern of relative motion between the three lenses and thus between the three images. If the substrate itself moved, it would have an identical effect on the 3 images, which is not a problem. Also, in the new design, the 3 images are focused on one single detector. The design had to be modified in order to fit the 3 beams in the micro lenses and in order to fit the 3 images on one single detector while maintaining the original plate scale. Table 1 summarizes the modifications of the design. Another advantage of the current design is that it is more compact. The distance from the relay lens to the detector is twice smaller than for the previous design.

	Previous design (3 separate lenses)	Current design (1 microlens array)
Relay lens EFL (at 450 nm) (mm)	152	100
Focusing lenses EFL (at 450nm) (mm)	86.7	38.5
Beam size at focusing lens (mm)	1.2	0.6
Distance Relay Lens – focusing lenses (mm)	250	112
Separation middle lens – top lens (mm)	10	4.5
Separation middle lens – bottom lens (mm)	5	2.3
Distance focusing lenses – detector (mm)	130	57
Plate scale at detector	0.236”sky/pixel	0.240”sky/pixel

Table 1: Comparison between previous design and current design

More details on the tip/tilt design can be found in a separate document.
DOC_6

4.4 Receiver Bench Tolerancing Analysis

An analysis was completed in order to determine the Surface Figure Error of the optical components on the Receiver Bench: Telescope PM, telescope SM, BCPM, BCSM, folds.
The analysis was a significant milestone. Based on this analysis we made a decision on the surface figure error of the telescopes, beam combiner, and folds. The analysis showed that the most critical components were the folds and the Telescope Primary mirrors. These optics have to be λ/20 wave RMS or better. After considering a compromise between cost and performance, it was decided to specify the telescope PM with λ/20 wave RMS. DOC_3

There is pinhole at the internal focus between the PM and the SM. This pinhole allows us to limit the field of view. An analysis was completed in order to determine the size of the pinhole showing that the pinhole should be at least 200 micron in diameter. A safe size is 300 microns. DOC_4

An analysis was completed in order to prepare the telescopes alignment activity in their GSE mounts. The analysis predicted the effect of PM and SM misalignment on the telescopes transmitted WFE (wavefront error). The results showed that angular misalignment is not detectable (WFE not changing) up to a few arcminutes. This means that it is not possible to optically align the telescopes mirrors within +/- 10” requirement (Error Budget) using the interferometric technique. Since there is no easy way to align the mirrors to that level of accuracy, the best option is to align the mirrors nominally parallel to each other assuming we can rely on the manufacturing data on the wedges of the mirrors. According to Nu-Tek, the

wedges are 6" and 10" respectively for the PM and the SM. So in the worst case, the misalignment between PM and SM would be 16", which is not far from the +/-10" requirement.

The analysis showed that the telescopes WFE is more sensitive to decenter misalignment than angular misalignment. However misalignment in decenter will not be detectable (WFE not changing) within the +/-10 microns requirement (Error Budget). The analysis showed that it will be very difficult to align the telescopes using the interferometric technique within the required +/-10" and +/-10 microns. DOC_5

4.5 TIPTILT SENSOR TOLERANCING ANALYSIS

A tolerancing analysis was completed. Initial alignment and stability tolerances were generated of each component of the tip/tilt sensor. DOC_6

4.6 SPECTROMETER

A tolerancing analysis was completed. Initial alignment and stability tolerances were generated of each component of the spectrometer. DOC_7

5.0 OPTICAL TESTING

5.1 TELESCOPES

The telescopes individual mirrors PM and SM, as well as the telescopes assemblies were tested at Nu-Tek and at GSFC. A summary of the measured figure errors is presented in a separate document "SVIP telescopes optical quality summary".

The Secondary Mirrors were slightly out of specification. But this defect was compensated by the Primary mirrors that were better than the specification. Overall, the combination of the Primary and Secondary mirrors resulted in System Figure Errors that met the specification.

The telescopes performance was re-measured at GSFC. The telescopes met the specification (surface figure error 0.050 wave RMS) when they were tested in the GSE mounts. However the performance of the telescopes was degraded (0.068 wave RMS) when they were tested in the composite mounts. DOC_8

A test activity was completed in order to measure the sensitivities of the telescopes mirrors misalignment. The telescope mirrors were in the GSE mounts and could easily be adjusted in decenter, despace and tip/tilt.

The results showed that the RMS WFE was very sensitive to despace (separation between the two mirrors on the z axis). A misalignment of 5 microns in despace (zygo power 0.140 waves) caused a change in the WFE from 0.056 to 0.060 waves RMS. We learnt that the mirrors have to be aligned to within ~ 2 microns in despace in order to minimize the telescopes performance degradation.

This activity confirmed that it was not possible to align the mirrors in angle by interferometry and that the best option was to align the mirrors parallel to each other using theodolites. DOC_9

5.2 BEAM COMBINER

A separate document presents the Beam Combiner testing. The results showed that the BC has a very good performance and meets the specification (Error Budget). DOC_10

5.3 MICROLENS ARRAY

The Microlens Array was tested using a Multiple Wavelength Dynamic Interferometer. The testing activity is presented in a separate report. DOC_11

6.0 MECHANISMS

6.1 MECHANISMS: SELECTION, CHARACTERIZATION, MODELING, AND TESTING

SVIP uses 6 mechanisms to provide a total of 9 controlled degrees of freedom. There is a tip/tilt mechanism and a delay line compensation mechanism for each of the three telescopes. The position of each actuator is controlled by feedback derived from the science camera in order to optimize the angle and optical path length of the light from each of the telescopes. Below is a table summarizing the performance required by each of the mechanisms, derived early in the development of SVIP:

Mechanism Type	Range	Resolution	Operating Bandwidth	Mounted Optic
Tip/Tilt	+/- 1 arcmin	0.05 arcsec	800 Hz	1" circle mirror
Delay Line	30 um	10 nm	800 Hz	1" retro-reflectors (2)

The combination of small range, very precise resolution, and stiff, high-speed operation led to the selection of piezo-based mechanisms. Finding a COTS solution was desired to reduce costs and development time. Since SVIP is a ground-based demonstration, and not a spaceflight mission, using COTS equipment was feasible. Physik Instrumente (www.physikinstrumente.com) was found to have products that met our requirements and priced within the SVIP budget. Below is a list of the items purchased for SVIP.

Qty	Description	PI Part#	Price Each
3	Tip/Tilt Platform +/-1mrad, integrated Strain Gage Sensors	S-330.10	$4,885
3	3-Channel Strain Gage Sensor/Controller Module	E-509.S3	$2,535
3	Linear Piezo Mechanism 38um Stroke, Integrated Capacitive Sensor	P-753.31C	$4,951
1	3-Channel Capacitive Sensor/Controller Module	E-509.C3A	$5,664
4	19" Rack-Mount Chassis with Backplane and Power Conditioning	E-500.00	$1,987
12	LVPZT Piezo Power Amplifier -20V to 120V, 200W	E-505.00	$1,893
12	LVPZT Extension cable, 5m	P-892.05	$75
3	Strain Gage Sensor Extension Cable, 5m	P-892.05	$104
1	Strain Gage Sensor Monitor Cable, 3 Channel	P-893K003	$130
3	Capacitive Sensor Extension Cable, 5m	D-892.05	$174
1	Capacitive Sensor Monitor Cable, 3 Channel	D-893.32	$130
		TOTAL	$75,435

Originally, the first units were purchased with a serial digital interface (RS-422). The mechanisms were characterized and found to operate to the correct range and precision, but the interface had inherent delays that prevented operation at sample rates of 800Hz. It was decided that the analog command input would be

used for providing the feedback signals from the DSP. This decision led to the purchase of the Multi-D/A Interface board, which is described in the electronics section. Figure 1 shows the delayed response to the digital serial interface and analog commands. The mechanism does not even start to move until 3ms after initiating a command, which was unacceptable for a 1.25ms command update rate. The step response to the analog command settles within 2ms before optimizing the piezo controller.

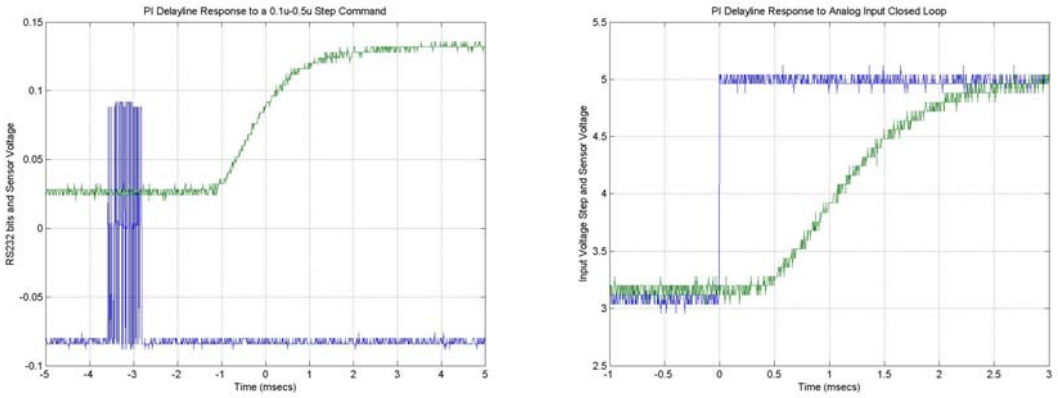

Figure 1: Sample Step Response Using the Serial vs. Analog Command Interface

Each mechanism has a built in sensor and therefore can be operated open loop (commanding the drive voltage to the piezo) or closed loop (commanding a sensor set point and using feedback to drive the mechanism to that position set point). Certain key parameters, such as slew rate and closed loop compensator gains can be adjusted using potentiometers on the control boards. To optimize the response of each mechanism, their optical loads were mounted and the electronics were tweaked. The open loop response was optimized by maximizing the slew rate of the drive amplifier. Step responses and sine sweeps were taken to determine how to adjust the notch filter on the controller to reduce excitation of the first resonance of the mirror inertia and piezo mechanism stiffness. The closed loop response was adjusted using the compensator parameters (proportional and integrator gains) to optimize the step response. Figure 2 shows the difference between the closed loop step response before and after the control parameter tweaking. Figure 3 shows the difference between the step response in Open Loop Mode and Closed Loop Mode, after the optimization procedure. It is clear that the open loop response is faster, but settles to a final position that is different than the commanded reference voltage. The closed loop operation is desirable because it provides a better correlation between command voltage and mechanism position. However, since SVIP uses the science to calculate errors in an external closed loop system, both modes would operate well in the overall system and be driven to the correct position to correct for disturbances. After tweaking, both modes now had settling times under 1ms, with the open loop mode settling in approximately 0.5ms.

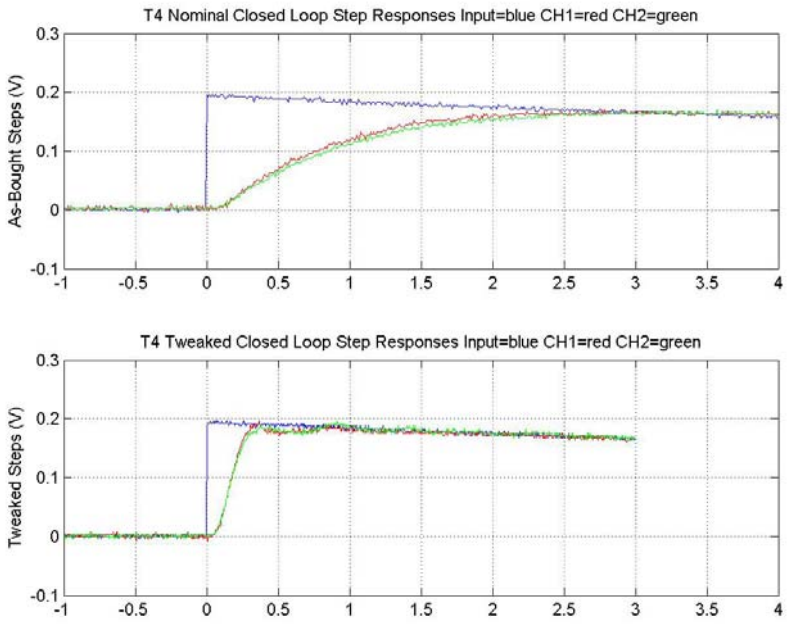

Figure 2: Step Response Before (top) and After (bottom) Tweaking Controller Parameters

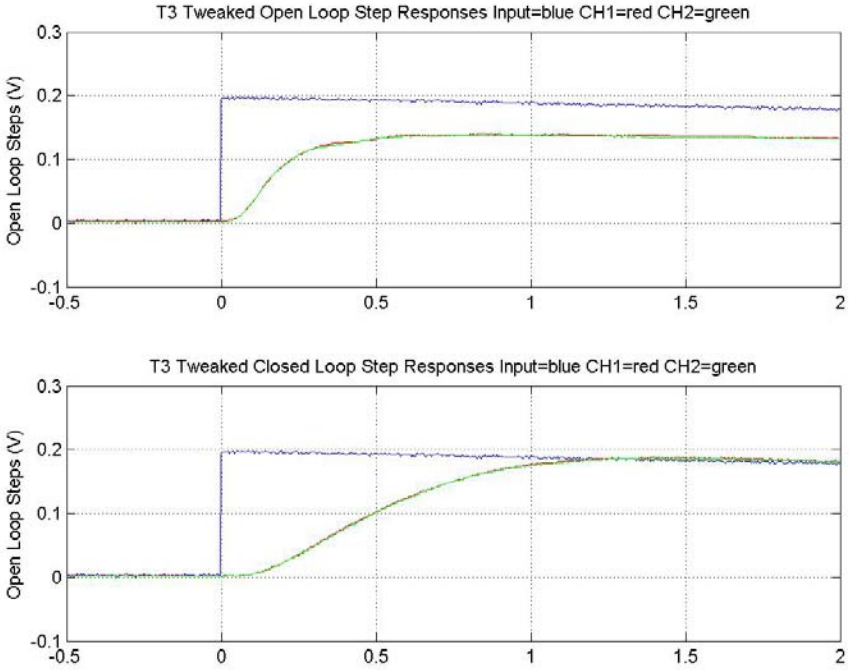

Figure 3: Open Loop (top) and Closed Loop (bottom) Step Responses After Tweaking Controllers

During testing, significant noise was noticed on the sensor output on several units. The sensor noise level was about 30 times higher than the published stability in the PI technical documentation. The PI data sheets claim a position stability of +/-0.5 urad. The noise on the sensor channels was about 8mV or scaled to 1.6urad. After several investigative tests and interfacing with technical people at PI, it was determined

that the cooling fans in the drivers were creating interference on the sensor electronics. This noise on the sensor signal was invariably fed into the closed loop system and affecting the motion of the mirrors. The fans act to cool the power transistors in the drivers, primarily for operating in high power conditions such as large displacements at high rates of speeds. Piezo devices are capacitive in nature and require large voltages, but very little current for low speed operation. Analysis showed that the corrections required for SVIP were on the order 100nm or 1urad at speeds up to 60Hz, and larger displacements over long time periods for thermal adjustments. Under these low power conditions, it was determined that the fans were not needed. In addition, the drivers include thermal shutdown circuitry to prevent damage. Therefore, the fans were disconnected on all the drivers. The noise levels reduced significantly, as shown in Figure 4. This concluded the initial characterization and optimization of the suite of SVIP mechanisms.

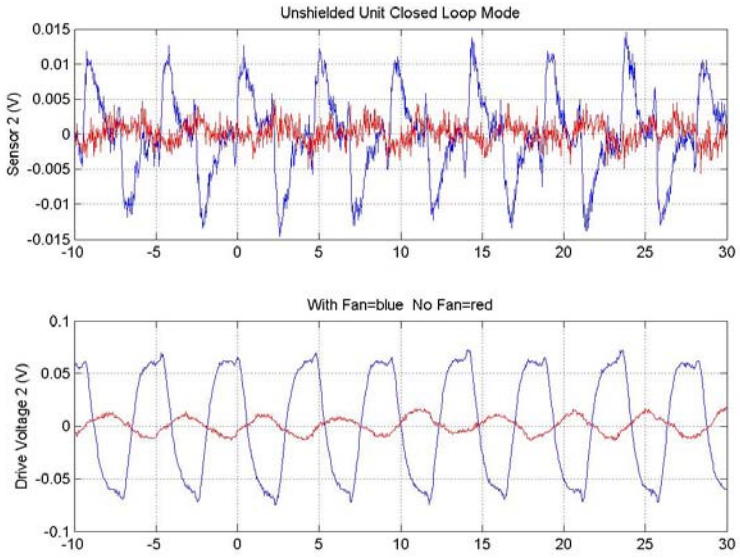

Figure 4: Sensor Channel (top) and Piezo Drive Voltage (bottom)
With (Blue) and Without (Red) Fans

Based on these test results, math models were developed and validated. The math models were combined into a system-level model to facilitate development of the overall SVIP controls algorithm and performance predictions. The math models were built in MATLAB/Simulink and were designed to capture all relevant parameters so any changes in hardware would be easily incorporated into the model. The parameters were based on PI data sheets and the characterization measurements in the time and frequency domains. Figure 5 shows the Simulink model for a tip/tilt mechanism, which is very similar to the model for the delay line. The following plots, Figures 6 and 7, compare examples of the measured step responses and frequency responses with the model simulations. There was very good correlation across the board. The complete data set is available electronically as part of this report.

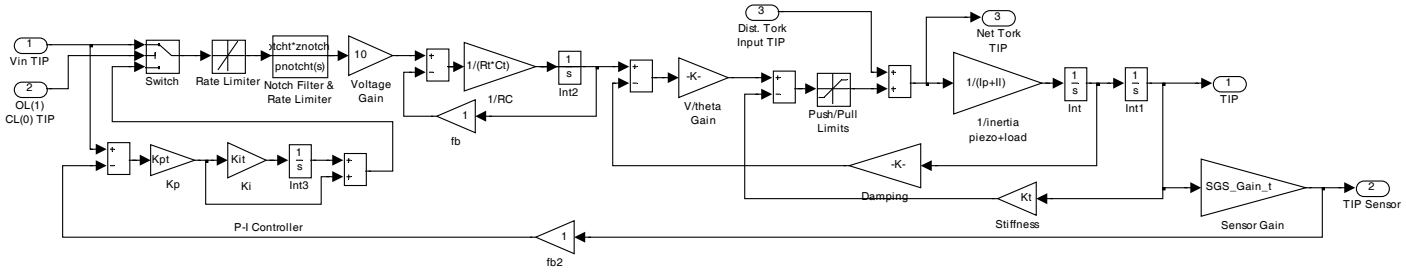

Figure 5: Simulink Model of 1-axis of a Tip/Tilt Mechanism and Controller.

The Tilt Axis and Delay Line Models Look Very Similar

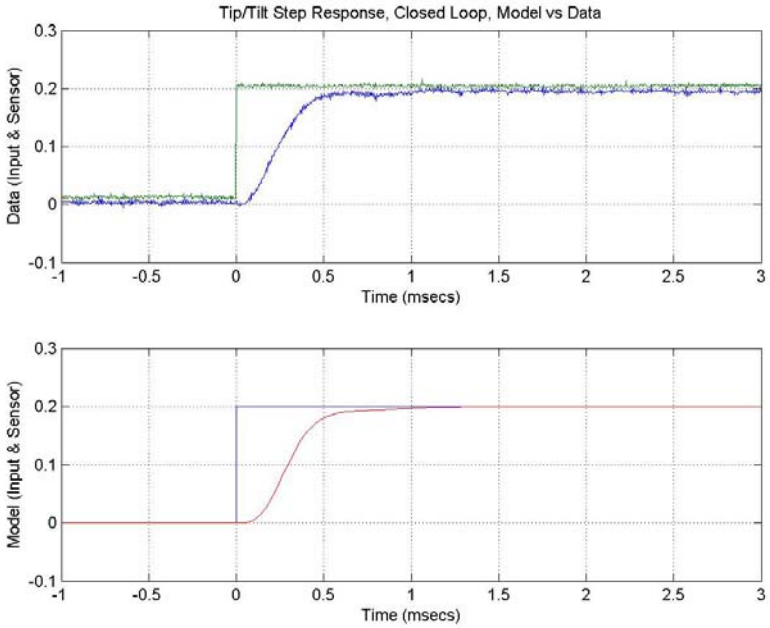

Figure 6: Data (top) and Model (bottom) Step Responses of a Single Tip/Tilt Channel Axis Operating in Closed Loop Mode

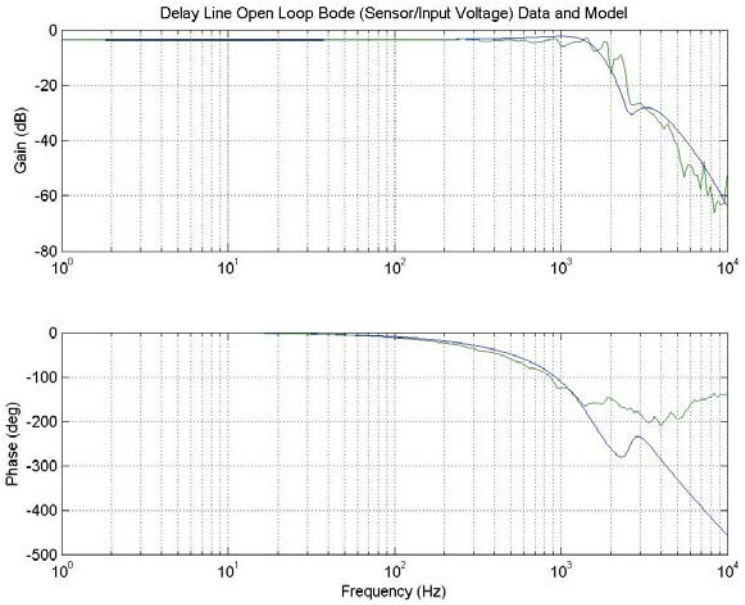

Figure 7: Data (green) and Model (blue) Frequency Responses of Delay Line Operating in Open Loop Mode

The individual mechanism models were then combined into a system-level simulation. The 800Hz sampling of the detector, which produces the error signals, was added and a variety of compensation filters were designed to stabilize the system at the highest bandwidth possible. The low frequency drift compensation algorithm was added as well. The algorithms used to determine mechanism corrections are described in Section XX of this report. The compensation filters designed for the SVIP controls loops would be added on the outputs of the error calculations and scaled properly to optimize the instrument

performance. After designing a stable system, the model was tested using simulated time data. Rick Lyon created 8 vectors of input noise that had the correct spatial and temporal correlations to simulate turbulence in the image processed by the detectors. This input noise was fed into the full, nonlinear system model to predict the amount of correction that could be expected out of SVIP. Figures 8 and 9 show the overall block diagram and some of the details of the various blocks in the controller section.

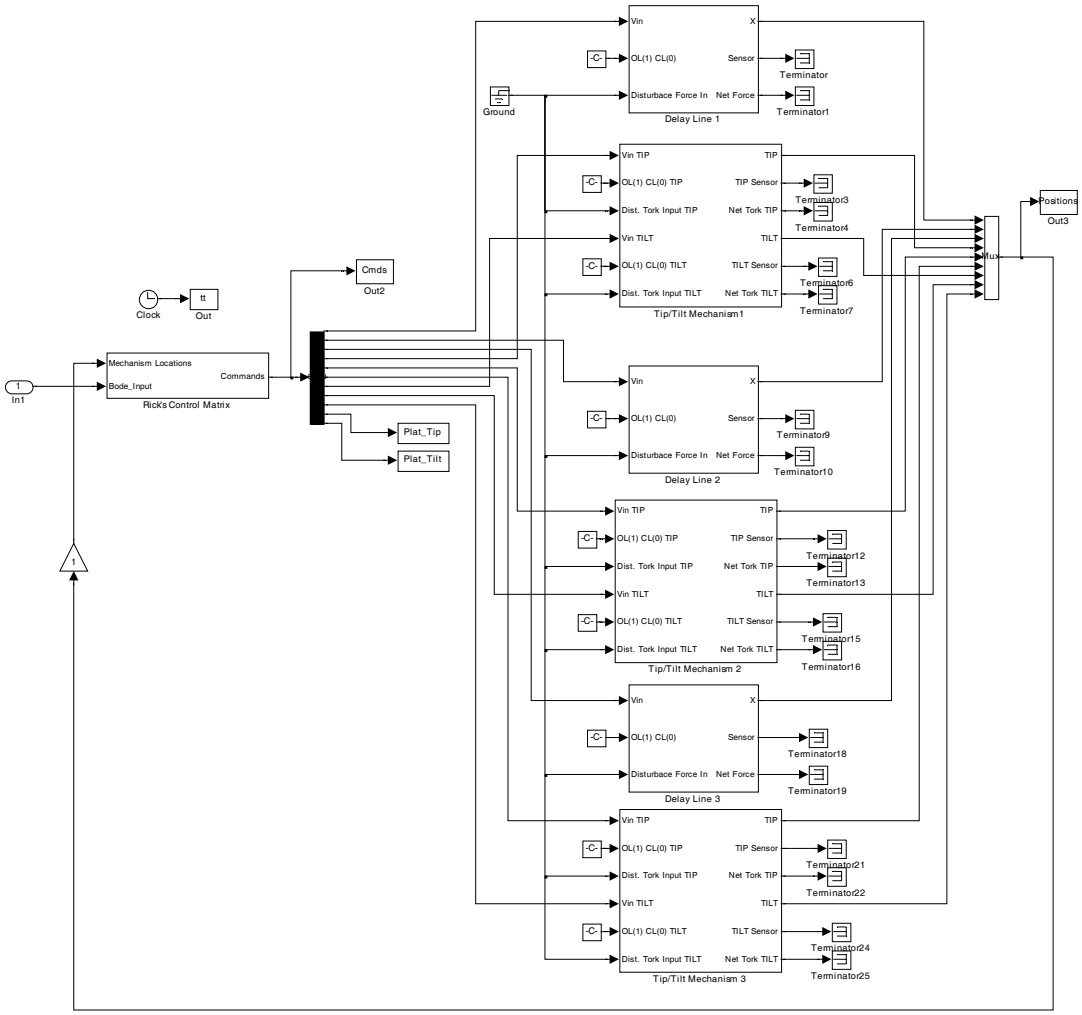

Figure 8: Simulink Model of Entire SVIP Correction Control System

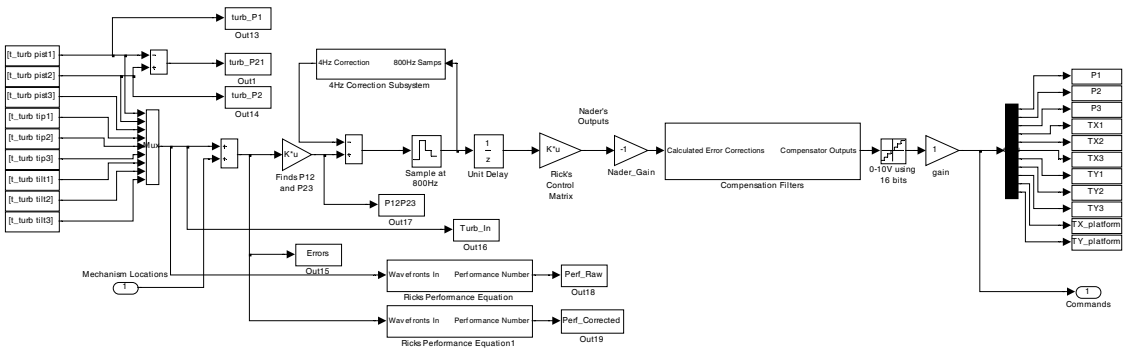

Figure 9: Simulink Sub-Block Showing Turbulence Inputs Various Image Correction and Control Algorithm Blocks

Figures 10 and 11 show some examples of the error produced by the simulated turbulence with, and without the correction. The spectrum results in Figure 10 show that there is significant correction below 20-30Hz, but the errors are actually amplified in some frequencies. At this point, it is believed that it is a result of the inherent time delays and phase shifts of a sampled-data system. A similar conclusion can be seen in the time response snapshot of Figure 11. The mirror tracks the lower frequency corrections, but is slightly out of phase with higher frequency corrections. While it indicates that the performance may not be optimal at turbulence frequencies up to 60Hz, this approach would very well for space applications in which the disturbance frequencies are significantly lower in frequency. This type or thorough modeling can be very useful as the instrument is assembled and integrated to aid in the controls development and save testing time.

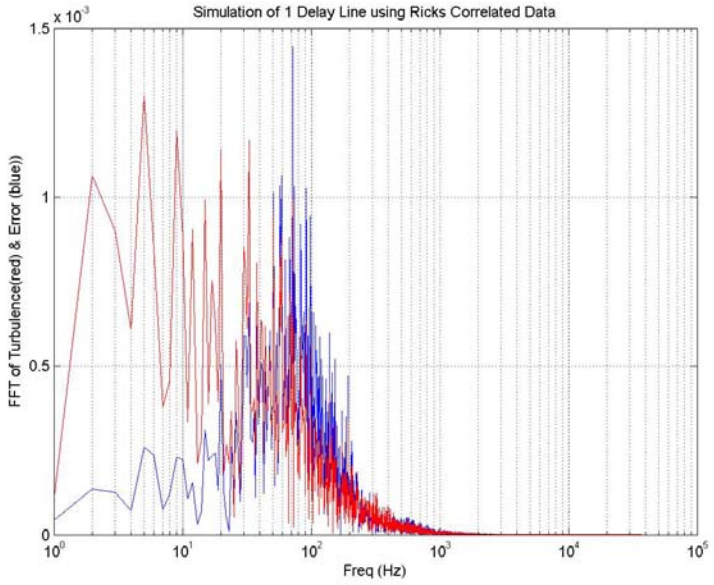

Figure 10: System Modeling – Spectrums of Turbulence and Tracking Error for One Delay-Line Axis. The Red Spectrum is that of the Input Turbulence, the Blue is the Net Error

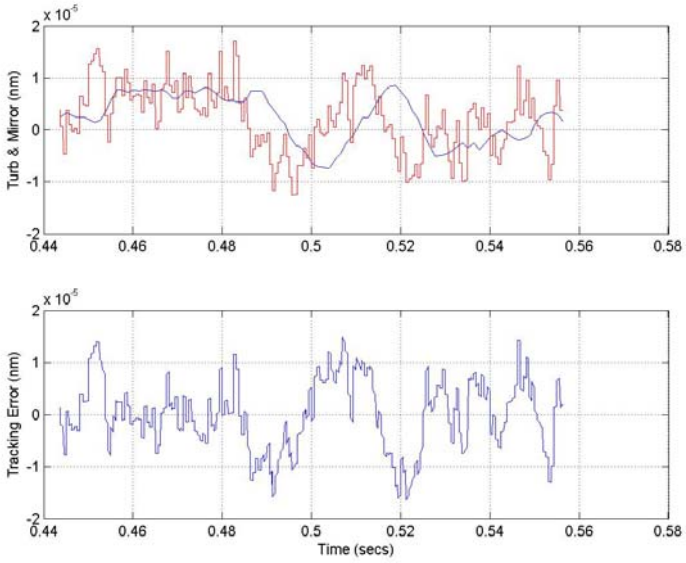

Figure 11: System Modeling – Time Series of Turbulence (top-red), Closed Loop Mechanism Response (top-blue) and the Net Error (bottom) of One Tilt Axis

When the mechanisms were characterized and the camera processing electronics were ready, a testbed was assembled to perform the initial testing of the closed loop, disturbance attenuation system. A laser-pointer was shot off of a tip/tilt mirror and then onto a camera. The image was processed, passed through the D/A converter board, and fed into the mechanism controller. First, an open loop system measurement was made by injecting a sine sweep into the mechanism and measuring the error signal processed. This data was used to again corroborate the model, and optimize a closed loop compensation filter. At this time, the camera electronics were being operated at 666Hz, rather than the full 800Hz rate. The sample rate is key to the digital filter parameters. Once the compensator was designed and included in the image-processing algorithm, the system was operated in closed loop mode to check performance. A second tip/tilt mirror was introduced into the optical path and excited to produce a known position disturbance. Using the first tip/tilt mirror, the error correction performance was measured. Figures XX – XX show the measurements made during this initial testing. Figure 12 shows the transfer function of the entire system. The sampling rate is apparent and appears as a notch at 666Hz. The sampling and processing delays appear as a phase lag, which tends to limit the maximum bandwidth of the system. Figure 13 shows the compensated, open-loop bode plot. The compensator was designed in MATLAB and the filter coefficients were programmed into the camera image algorithm. Figure 14 shows the net closed loop bandwidth of about 60Hz with virtually no peaking, which indicates good phase margin. These results matched well with the model and show that the image correction subsystem is functioning and stable.

At this time, the mechanisms have been integrated into the instrument bench and the optical system is being aligned and characterized. The mechanisms have been operated by hand to help in this process and seem to be operating nominally. When the entire system is completed, the mechanism loops can be operated and the final closed loop filter parameters can be selected.

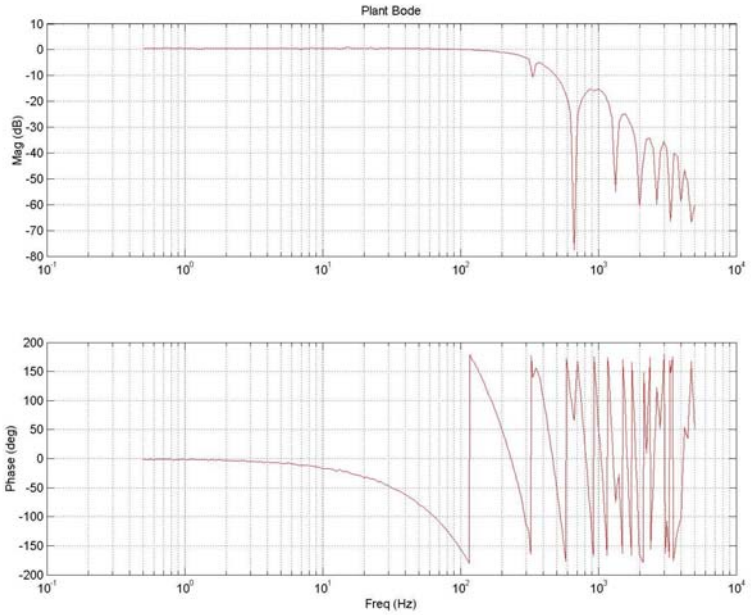

Figure 12: Measurement of Tip/Tilt Response Using Camera Testbed as Feedback

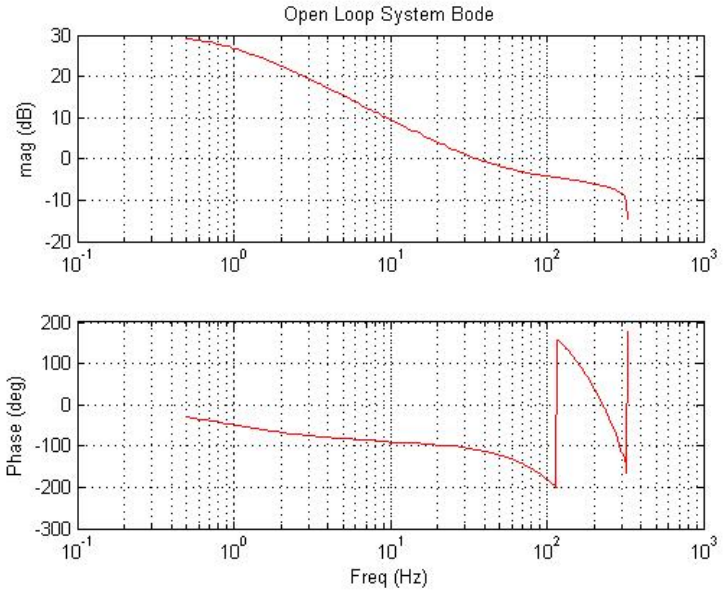

Figure 13: Open Loop System Response After Compensator was Design and Implemented

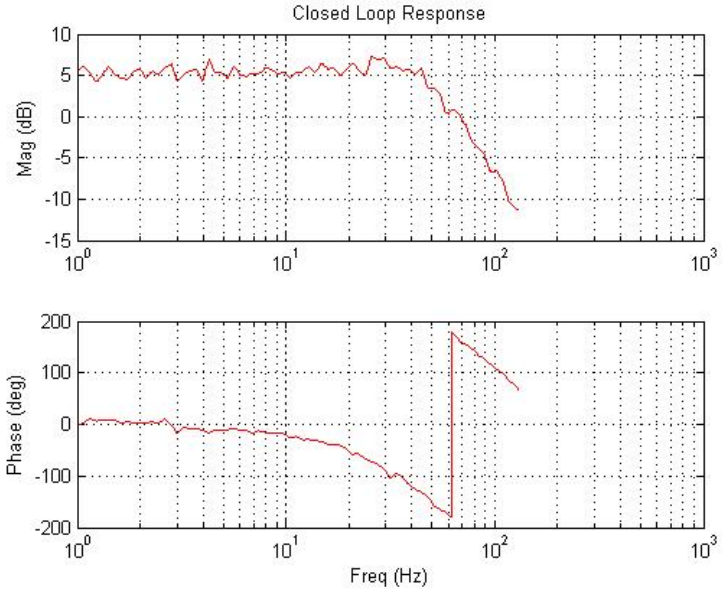

Figure 14: Closed Loop Testbed System Showing About 60Hz Bandwidth using 666Hz Sampling Rate

Lessons Learned:

- Carefully characterize COTS hardware. Very often it can be significantly improved.
- Detailed modeling is a useful tool that can predict behavior and allow analysis and optimization to be done prior to expensive hardware testing.
- Correlate the model with test data at each step in the development process.
- Camera sampling and image stabilization/correction can be performed at 666Hz using the image sizes adequate for solar science.

7.0 MECHANICAL DESIGN

7.1 MECHANICAL DESIGN OVERVIEW

The mechanical structure of SVIP is required to support three telescopes spaced at 40 cm. and 80 cm. apart center-to-center on a dimensionally stable boom as well as support the associated optics, mechanisms and detectors to demonstrate the wave front sensing and control goals. In addition, the entire structure needs to mount to a 2-axis solar tracker for performing measurements while tracking the sun and selected celestial targets.

After several iterations of the optical design and resultant updates to the error budget, it became clear that it would be nearly impossible to assess the relative sensitivity of each individual optical element and derive a stability requirement given the system complexity and the limited time available. With that in mind, we chose an approach that would give us the maximum mechanical stability and robustness within our budget allocation. Since the mechanisms can correct for small motions in the 25-30 micron range, the primary goal was to maintain all optical elements on the optical bench to a total RSS of less than 25 microns over 20 degrees C, and throughout all gravity vector orientations. Therefore, the driving design considerations included: stability and co-alignment of the optics, cost, schedule, desire to minimize overall mass for handling and field testing, and packaging for mount on a commercial OTS solar tracker.

During the first year of the study, the initial baseline design was:

- Structure designed for 25 to 50 Hz.; goal to show WF sensing system can accommodate structural modes (scalable to flight mission EASI)
- Kipp-Zonen solar tracking platform selected as baseline pointing-tracking system; 3 month availability, accommodates 130 pounds, accurate to a few arc seconds pointing.

- Composite face sheet – aluminum honeycomb core optical benches were chosen for stability, cost, flexibility, fabricability and mass considerations.

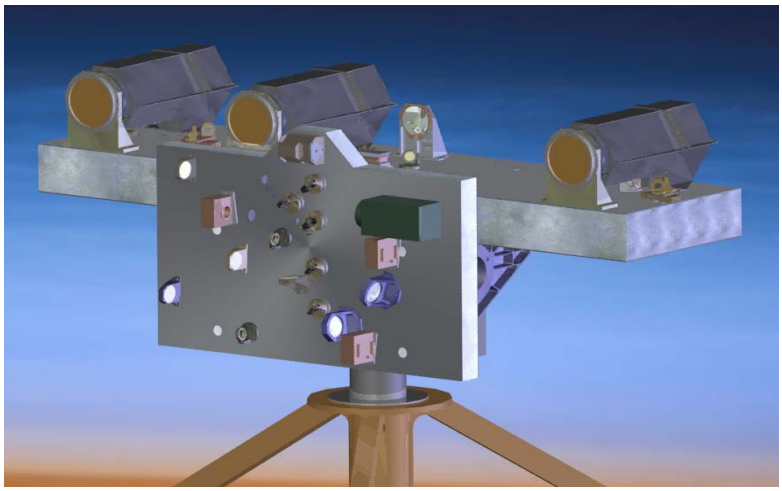

Figure 15 An early design of the two bench layout

Following a more detailed mechanical analysis with Finite Element Modeling (FEM) we redesigned the mechanical packaging to incorporate a stiffer structure design while keeping the optical bench panels the same size. The rationale behind the repackaging effort was:

- The air turbulence knee frequency is around 50 Hz. so we would prefer to either be above or below this to decouple the modes.
- After evaluation of the available OTS mechanisms, only smaller range piston mechanisms (38 um range) vs. (100 um range) would meet the bandwidth and cost requirements. Smaller total correction range requires that the boom deflect less, therefore driving towards stiffer structure.
- A less expensive and more robust solar tracker became available (different mechanical interface).
- Additional refinement of the closed-loop error budget resulted in a better understanding of the component interactions. Stability and relative co-alignment of the three aft detector channels is also important to minimize non-common path error disturbances. The new “bi-plane” design minimizes bench sag, torsion and bending modes and results in better overall mechanical stability.

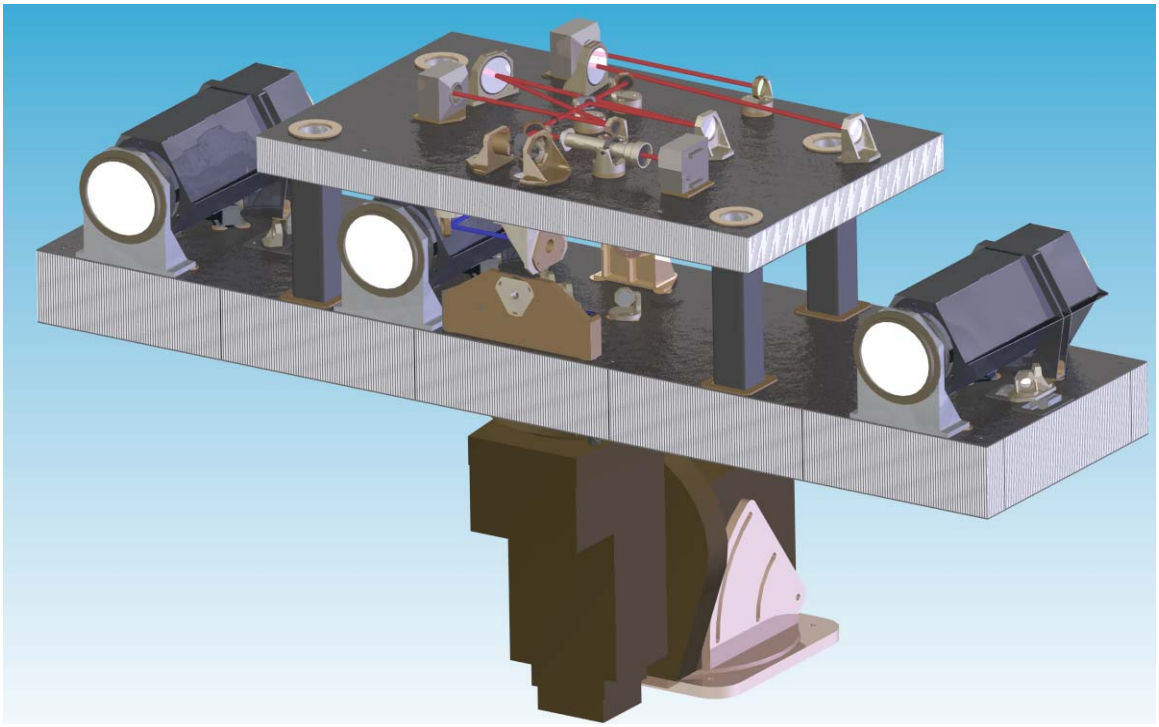

Figure 16 The final design of the two-bench layout that is more stable.

7.2 Analysis and Finite Element Modeling

A detailed FEM was developed to assess critical aspects of the SVIP mechanical design. Gravity loading and temperature swings (20 degrees C) were used to assess system performance. The overall goal was to achieve greater than 110 Hz., less than 20 microns of deflection in all degrees of freedom and maintain optical element co-alignment to 10 microns.

A detailed summary of the FEM analyses results are included in the appendix for reference. The final design achieved a predicted 118 Hz. and less than 10 microns of relative motion of all elements under thermal and gravity loading.

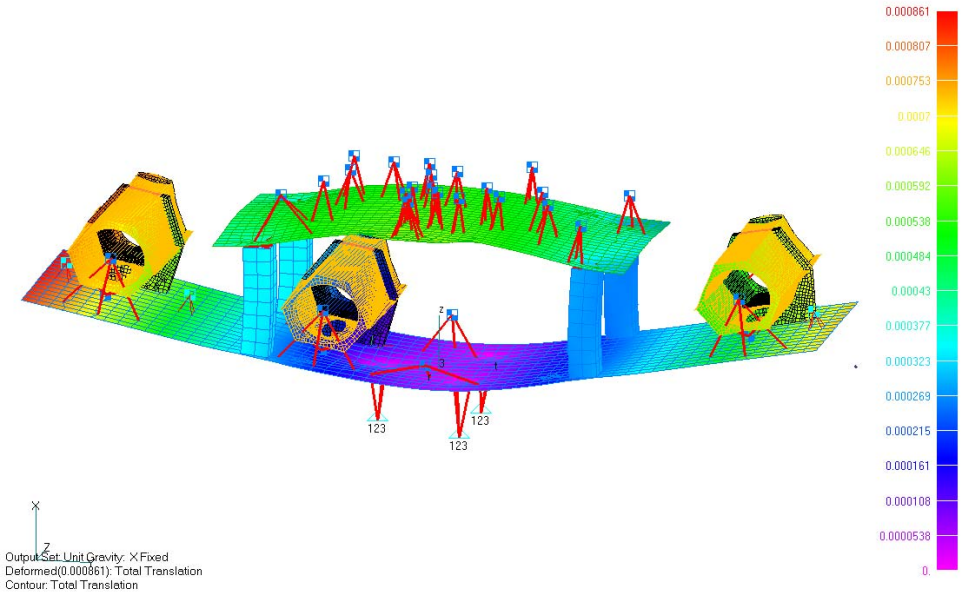

Figure 17 A dynamical analysis model of vibration modes

7.3 Solar Tracker

Figure 18 Solar tracker capable of supporting 150 pounds

The solar tracker selected and purchased for SVIP is an OTS Paramount ME German Equatorial Robotic Telescope mount, purchased for approximately $13 K. The Paramount ME is well suited for SVIP with a performance of better than 5 arc-seconds between corrections and the ability to handle up to 150 pounds (SVIP is approx. 100 pounds). Electrical interfaces allow for control either with or without the SVIP electronics in the feedback loop, allowing the user to operate in a GOTO mode or in a closed loop feedback mode.

The tracker, the titanium interface plate and the SVIP instrument are all separable for ease of handling, shipment and set-up at observation sites.

7.4 Optical Benches and Structural Interfaces

The SVIP optical benches are comprised of Quasi-Isotropic M46J composite face-sheets with low density aluminum honeycomb core and titanium component inserts. The table below shows the materials used for the key structural components.

Receiver Bench	M46J, QI, 0.08" thick facesheet, 4" Al.5056 3.1 p.c.f. core
Detector Bench	M46J, QI, 0.06" thick facesheet, 2" Al.5056 3.1 p.c.f. core
Corner Support Struts	M55J, QI, 0.090" thick walls, 2" square tube
Telescope Tubes	M46J, QI, 0.040” thick, locally stiffened at interfaces
Tracker Interface Plate	Titanium 6Al-4V, 1” thick

Over 20 degrees C temperature swings and multiple gravity vector orientations, Finite Element Modeling (FEM) showed that the design could easily meet requirements and would be inexpensive to implement. Face sheet materials were fabricated in-house at GSFC in the composites development lab from spare flight M46J pre-preg material. Both optical benches were consolidated in the lab and insert installation was performed using precision tooling. By utilizing CNC programming and precision flatness off-the-shelf MIC6 tooling plate, we were able to locate all of the component mounting inserts to within 0.001" to 0.002" and relative co-planarity and flatness to 0.001". This fabrication approach was extremely cost effective and the net result was an inexpensive precision optical bench.

SVIP Optical Benches	Labor Hours	Cost
Composites Layup and Cure	40	$ 3,200
Bench consolidation and Cut/routing	16	$ 1,280
Tooling plate machine holes	16	$ 1,280
Titanium spool inserts (approx. 40)		$ 3,000
Bonding of inserts into bench	8	$ 640
Inspection, CMM	5	$ 400
TOTAL OPTICAL BENCH COST		***$ 9,800***

More detailed design information and fabrication photographs are included in the appendix.

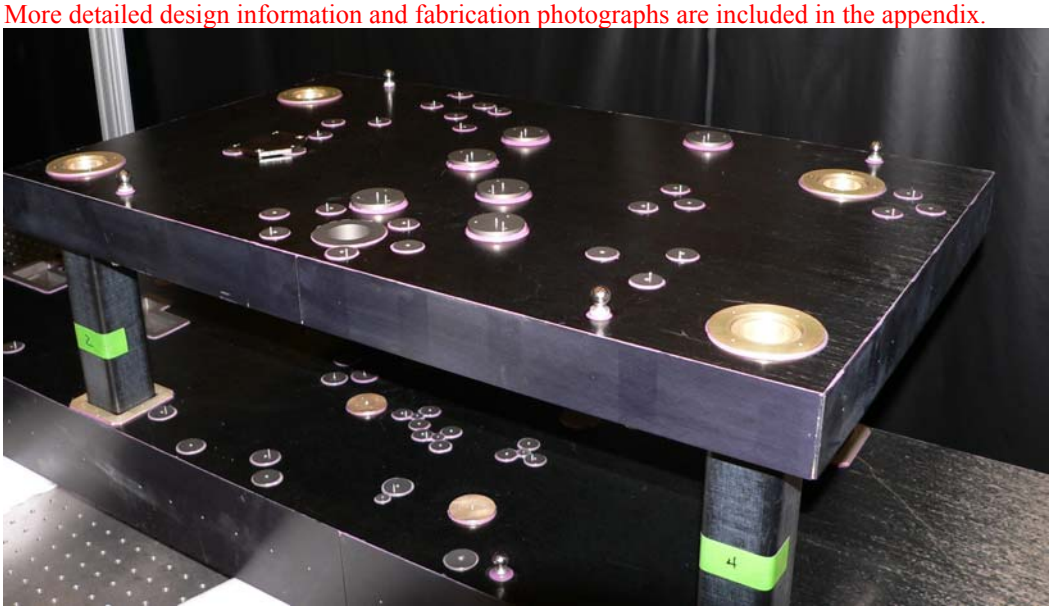

Figure 19 The SVIP receiver and detector optical benches

Critical to the overall mechanical stability are the structural interfaces. These interfaces are:

- Receiver Bench to Detector Bench
- Benches to Solar Tracker
- Optical Elements to Benches

7.4.1 RECEIVER BENCH TO DETECTOR BENCH: The two optical benches are coupled together with four corner posts as shown in Figure 19. Finite Element Modeling was used to optimize the cross-sectional area of the four corner posts for stiffness given geometry restrictions of the existing instrument layout. We were extremely fortunate in that the calculated post size almost perfectly matched existing spare square tubing from the SWIFT flight program. The spare M55J, quasi-isotropic 2" square tubes with 0.090" walls were well suited to application on SVIP and were available at no cost to the project. Some titanium

end plug fittings were designed to bond to each end of the tube and a flat/cup/pin arrangement was used for a tight, repeatable interface between the benches. One important consideration to note in the interface design is the importance of the load paths being tied to both face sheets, both at the bench-tube-bench interfaces and also at the solar tracker interface. All of the higher load fittings are "through the thickness" inserts rather than face mounted inserts which significantly increases overall system stiffness.

7.4.2 BENCH TO SOLAR TRACKER: The SVIP instrument interfaces to the solar tracker via a stiff titanium adaptor plate that attaches to the three primary instrument mounting inserts. The adaptor plate was optimized and fabricated for SVIP and is not part of the commercial tracking platform. We used the adaptor plate as the bonding tooling/template to ensure that the three instrument-mounting points were co-planar to the plate and no distortions would be induced upon mating and torquing the instrument to the tracker.

7.4.3 OPTICAL ELEMENTS TO THE BENCH: Optical components, detectors and mechanisms are very low mass and flange bonded inserts are sufficient to maintain stiffness and stability. All component mounts have a provision for liquid pinning each element to the optical bench after final alignment. The SVIP component mounting inserts have integral pins that slide into oversized holes on the mating component. After final alignment is achieved and no further adjustment is required, the gap between the pin and the hole are filled with a stiff epoxy to ensure extreme stability during field operations and handling. This type of liquid pinning approach has been proven successful on many flight missions and is a simple method to maintain alignment. Should temperature and vibrational loads cause a loss of preload due to insufficient torque, the liquid pin carries the shear load and keeps the component in position.

7.4.4 OPTICS MOUNTS: As mentioned previously, the overall mechanical system implementation was driven by the need for highly stable optical mounts and system pointing to avoid corruption of error signals. Rather than performing detailed opto-mechanical analysis on each of the many elements, we utilized best practices from experience and matched the metallic CTE (coefficient of thermal expansion) to the optic CTE. As such, the optical mounts for SVIP are made of either invar or titanium, depending of the optical element material; invar is used for supporting zerodur and fused silica optics, and titanium is used for supporting BK7 optics. We found that fabrication with titanium and invar was not significantly more expensive than with aluminum and provided additional stability that eventually saved time during integration and alignment. In addition, all optics on SVIP are bonded into their respective mounts to increase optical stability for outdoor testing.

7.5 RECEIVER TELESCOPE MOUNTS

Early on it became obvious that one of the critical components of the system performance was the stability and co-alignment of the three receiver telescopes. Through sensitivity and error budget analysis we derived a stability specification of 5 um and 5 arc-seconds for each telescope system. This requirement drove us to the need for packaging each telescope in a sub-assembly stable housing to preserve relative co-alignment of the primary and secondary mirrors over temperature excursions and gravity vector changes. After considering several options, the most cost effective and efficient design was a GSFC in-house built composite hex-tube. A Finite Element Model was created to optimize stiffness and ensure co-alignment and stability of the tube. The final design weighs less than two pounds including the metallic fittings and supports three pounds of optical elements while maintaining pointing and relative position to approximately 1 um.

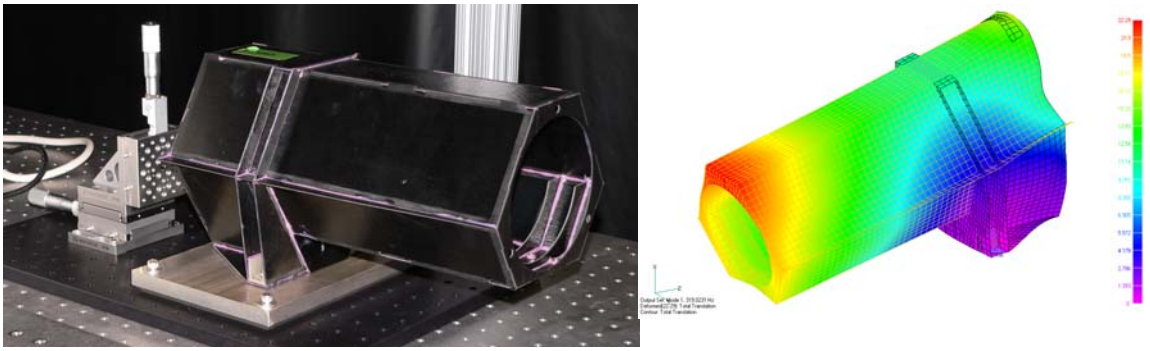

Figure 20 The carbon fiber telescope hex-tube (left) and stiffness model (right)

The same spare M46J material used for the optical benches was layed-up in a thinner (0.040") QI sheet. The entire hex-tube is created out of one piece of 0.040" flat stock material that is cut into pieces and the tube is then bonded into shape with a simple tooling fixture. The same bond fixture was used to assemble each tube, ensuring uniformity between the three assemblies. Photos below show how all of the hex-tube pieces were routed out of one piece of composite laminate.

Figure 21 Pre-assembly parts for the hex-tube (left) and the assembled tube (right)

The technique just described proved to be very cost effective and also highly stable and stiff. During the last six months of alignment and testing on SVIP, the aligned telescope assemblies have been handled and moved to a variety of set-ups, none of which resulted in loss of alignment. The fact that we have done optical performance sensitivity testing on the un-mounted telescope optics and know how exactly how sensitive the system is to decenter and despace errors, we have been extremely pleased with the long term stability and performance of these composite mounts.

7.6 DRAWING AND PARTS SUMMARY

SVIP consists of a total of over 450 fabricated and purchased parts. As described above, we utilized best practices in considering overall opto-mechanical design and performance. Appendix M1 contains the 161 mechanical fabrication drawings with all the detailed specifications of the parts.

Mechanical appendices:

Appendix M1 : pdf file with the 161 mechanical drawings (SVIP detail drawings.pdf)
& FEM analysis summary (file name is mechanical appendices final report.doc)

Appendix Fabrication and assembly photos (mechanical appendix photos.doc)

8.0 Electronics and Detectors

Scientific requirements:

Sensing and correcting for the effects of the atmospheric turbulences and boom dynamics on the three SVIP telescopes, requires a close loop control in real time of the optical paths and the acquisition and processing of video data from three synchronized high speed cameras at rates up to 800 Image/second from each camera.

Time for :(Image Acquisition + Image processing+ Control of the optical paths should be done in less than 1.025 ms.

The 800 Hz image acquisition rate requirements has driven the selection of the SVIP electrical parts and set the components specification to a high level pushing the edge of current off-the-shelf technology. We were very successful, not only in identifying commercial parts at a reasonable price, such as the high-speed cameras, high fidelity piezoelectric actuators, but also in testing a new generation of control algorithms using high-speed computation and data transfer technology equipped with the latest generation of programmable chips and digital signal processors. We were able to finalize an innovative electrical design and demonstrate that new technology capabilities can be used to achieve SVIP design requirements.

Using an novel design that incorporates multiple digital signal processors (DSP) working together in a parallel processing mode and programmable chips (FPGA) to stream the data from the three high speed cameras (800 image/s from each camera) has not only accelerated the SVIP development process, simplify the hardware design but has also provided a cost-effective approach for testing the closed-loop control circuits needed for the instrument's adaptive optics.

Data Rates

Camera 1 (WFS)	**1280*270 *800 frames**	**= 276.48 Mbytes/s**
Camera 2 (DFS)	**1280*128*800**	**= 131.072 Mbytes/s**
Camera 3 (DFS)	**1280*128*800**	**= 131.072 Mbytes/s**

Total of		**538.624 Mbytes/s**

Processing such amount of data within the 1.25 ms timeframe is unfeasible using a PC or even a workstation. For this reason and since the early stages of the SVIP design and development, our efforts were oriented towards the High-speed Digital Signals Processing platforms.

SVIP Bloc Diagram and data Flow:

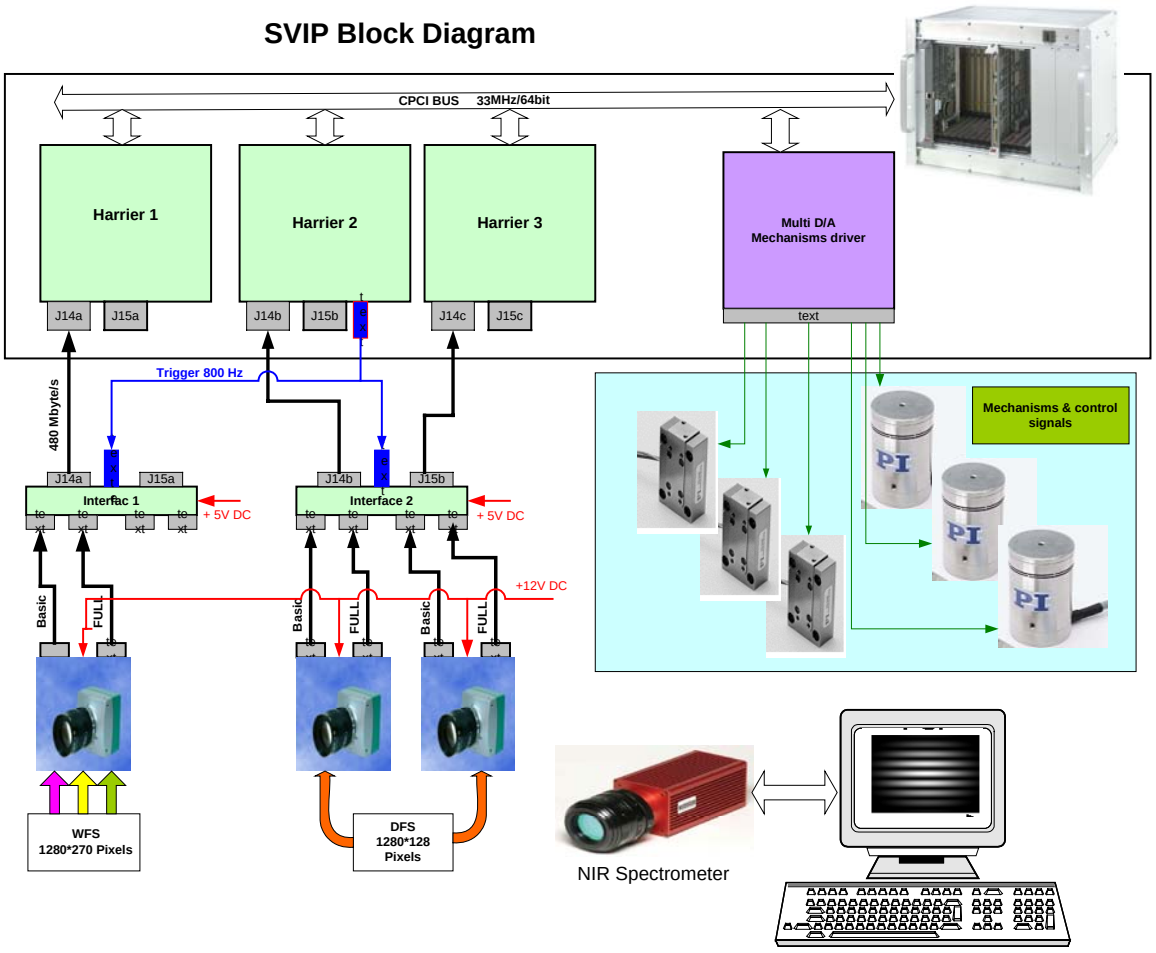

Images acquired by the 3 High speed Mikrotron cameras (one for the Wave front sensing and two for the Dispersed fringe sensing). Are transferred to the corresponding processing unit. Each of the three high speed COTS processing units equipped with 15 high speed Digital Signal Processors (Texas Instruments TMS320C6415 running at 600 MHz) providing a sufficient computational power to achieve the system processing requirements stability. Each unit is also equipped with 5 FPGAs configured as a camera link interface allowing a high fidelity transfer of the video data from the visible cameras into the DSP external memory thus increasing the system capability by managing the distribution of the image data on the 15 digital processors for the parallel processing. One of the Processing units is configured to generate the trigger signals to the cameras, permitting the synchronization of the image acquisition from the three cameras.
Once the processing is done the digital results are transferred to a host PC through a high speed compact PCI Bus. The PC receives regularly a status report from each of the processing units. The PC will then communicates processing results to Multi Digital to Analog converters. Digital values are then converted by the Multi D/A board into analog signals that will be used to continuously drive the five piezoelectric mechanisms.

The Near Infrared sensor will acquire the spectral images at a lower rate (5 Hz) giving the time to the system to achieve stability. Images for the NIR camera will be saved on the PC

SVIP Electrical hardware:

Visible Cameras(Mikrotron)

camera is equipped with a configurable window size CMOS image sensor, 1280 × 1024 (1.3 Megapixel) and pixel size of 12 × 12 µm , well capacity of 63000 electrons. The onboard 1280 Analog to digital converters and 10 output ports it is possible to achieved an output data rate up to 660 Mbytes.

Harrier Board (MangoDsp

Is one of the most powerful COTS boards in the market. It's high flexibility in image manipulation (size, position, and frame rate, preliminary processing….). has certainly minimized the SVIP hardware development. Each board is equipped with 15 fixed point digital signal processors from Texas instruments (TMS320C6415 / 600MHz) and 5 FPGA configured as a Camera link interface with data transfer rate up to 660 Mbytes.

Host PC

The PC represents the high level user interface. It provides access to the hardware init, operation and control functions, image download and acquisition synchronization. This module is the SVIP system watchdog, since it will supervise the background tasks (access to the shared memory), and data transfer through the main cPCI bus by the different DSPs and the control signals of the multi DAC board.It will keep a history and status file that can be used for hardware& software debug and stability evaluation.

Multi digital to analog board by ICS_ltd.

Due to the considerable time delay of the mechanisms digital interface, we were forced to drive the piezoelectric mechanism using its standard analog input command. For this purpose we have chosen ICS 725 for its high resolution, speed and programming flexibility. The ICS has can provide up to 32 independent and synchronized analog signals. The DAC resolution 16 to 24 bits and it is software

NIR Camera (Sensors unlimited)

This is a high Sensitivity solid-state InGaAs image sensor 640 x 480 pixel resolution on 25 mm pitch and a programmable exposure times > 50 ms Room temperature operation and integrated thermoelectric cooler. This cameras is equipped with a low noise 14-bit A/D and a digital Camera Link® compatible output

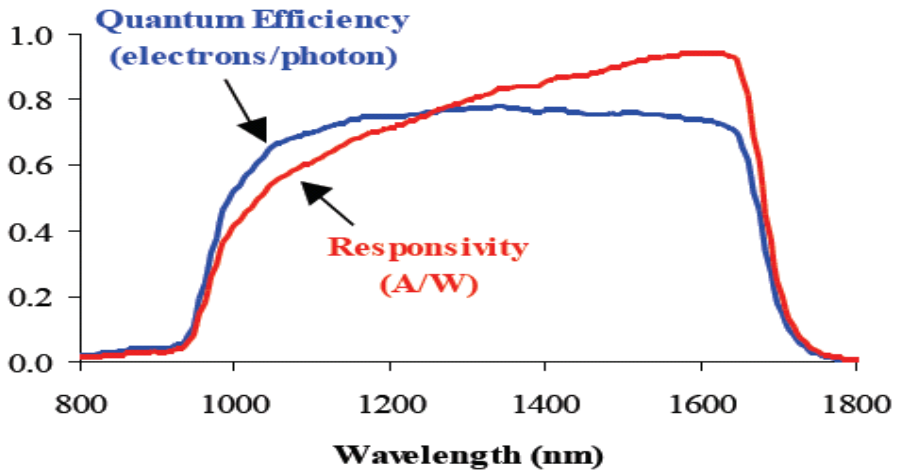

Software Development

The close loop control of the system is based on operation of two algorithms, the Tip/tilt algorithm and the Dispersed Fringe sensing algorithm. Both algorithms has been successfully developed and implemented into the processing units.

The tip/Tilt algorithm is based on a two dimensional FFT(DFFT), and the processing sequence
Three processors were able to share the processing of the image sequences was chains were Broken into three stages

- Processing the rows of the matrix, which is stored in the DSP external memory.
- Reorganizing the result of step 1 so that columns of the matrix are stored contiguously in memory.
- Processing the columns of the result of step 1 but on a reduced size window.

The 2DFFT is realized on each of the images from the three telescopes then the cross correlation is calculated in function of the reference image.
The Dispersed Fringe Sensing algorithm is straightforward. A liner fitting fitting is realized on both images (sliding window) then the delays are calculated from the differential pistons between each telescopes

Lessons Learned :

The data transfers between the processing units and the D/A board represented the major challenge for the SVIP electrical design and an important bottle neck. By allowing the D/A board to share the cPci bus with the host PC and the processing units, the time delays and became considerable and limited the system speed to 530 image/s. The recent parallel processing library that has been recently integrated into the system is expected to boost the system efficiency up to 600 image/s.
This problem can be solved by improving the speed of the digital interface of the piezoelectric mechanisms thus eliminating the need for the D/A board. Another possibility to resolve this issue is by building a custom designed D/A board that with the capability to communicate with the processing units through the FPGA instead of the cPci bus..
- A second generation of TI high speed DSP 32C6416, became available while we are in the final stage for the SVIP development. These processors have clock frequency of 1 GHz instead of the 600 MHz used for the TI 6415 SVIP In addition to a number of improvements in its architecture and functionality. Such a device can considerably increase the efficiency of the SVIP.

9.0 Algorithms and Control
RICKS STUFF HERE …

10.0 ALIGNMENT, INTEGRATION AND TESTING

10.1 INTRODUCTION

This section describes the alignment flow baselined for SVIP and documents the current status the instrument. The chart shown below (*fig. #1*) depicts the proposed alignment plan. However, it does not factually represent the work performed to date. Departures from this plan along with the accompanying rationale are presented in the sections that follow.

SVIP Integration and System Alignment Flow

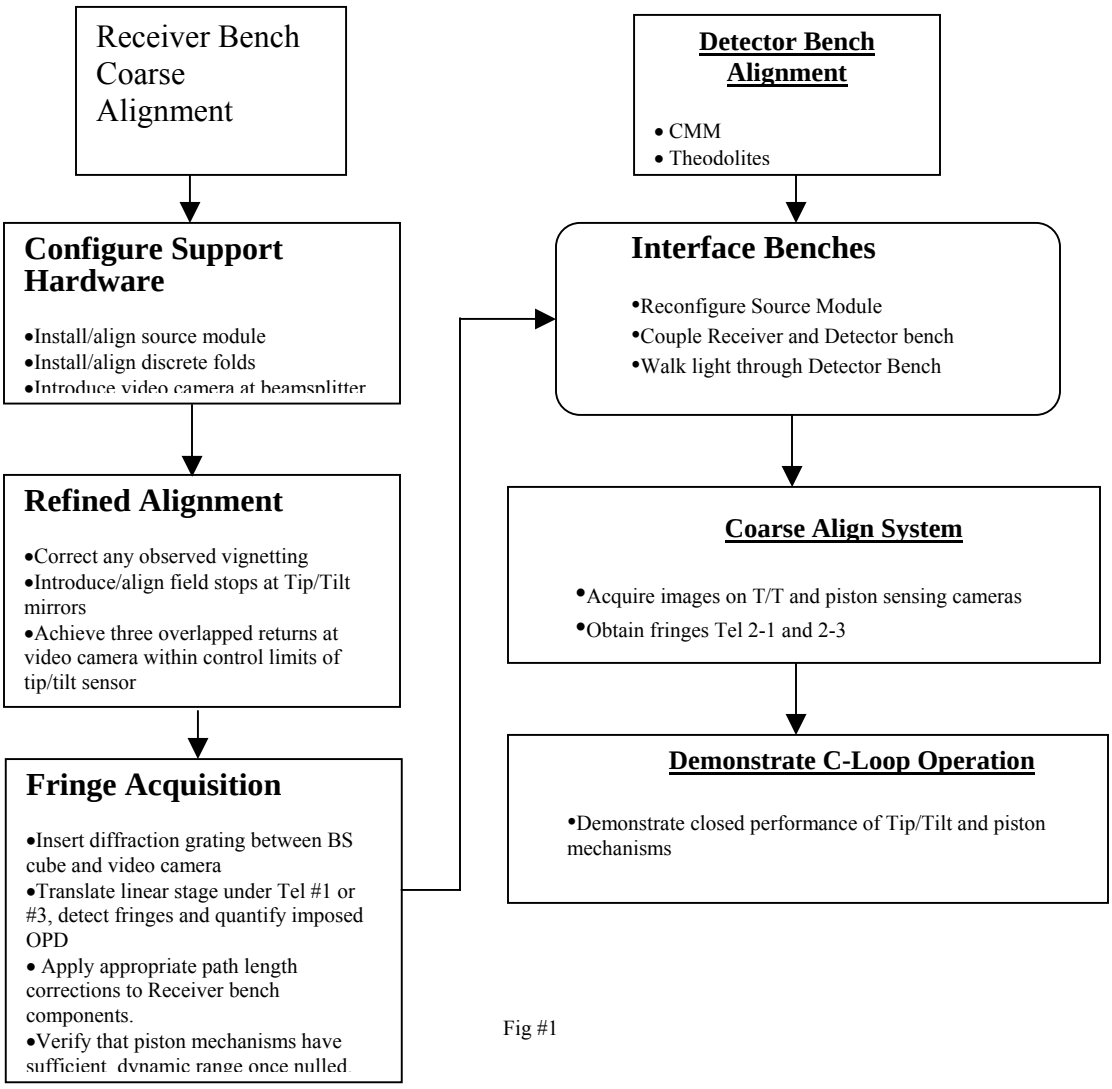

Fig #1

*Dispersed Fringe Sensor (DFS)

10.2 RECEIVER AND DETECTOR ASSEMBLY/ALIGNMENT:

The receiver and detector benches were coarse aligned using a Coordinate Measuring Machine (CMM) along with conventional theodolite metrology. The CMM was used to establish the despace between optical components while theodolites were used to set azimuth and elevation. At this phase of the alignment, each optical component was set to its nominal position and angle as prescribed by the optical model. Elevation angles were measured with respect to gravity and an alignment cube served as the Primary Azimuthal Reference (PAR). The specifics of this alignment are described in section 5.0 of this document.

10.2.1 SVIP SOURCE MODULE PHASE #1 (RECEIVER BENCH ALIGNMENT):

The Source Module (SM) was developed to provide point source illumination for the SVIP beam combiner secondary mirror. The SM consists of a light source, spatial filter assembly, beamsplitter cube and a video camera. The SM is positioned on axis with the BC secondary mirror so that the plane of the pinhole (~25um) lies at the focus of the BC.
In this configuration, the SM presents an on axis, spatially filtered point source to the BC secondary mirror. In addition to injecting light into the system, the source module allows the PSFs of all three SVIP telescopes to be imaged onto the video camera. This feature allows the alignment and phasing (with external DFS*) of the three telescopes to occur independent of the detector bench. The subsequent co-alignment of the receiver and detector optics is simplified with a pre-aligned receiver bench.

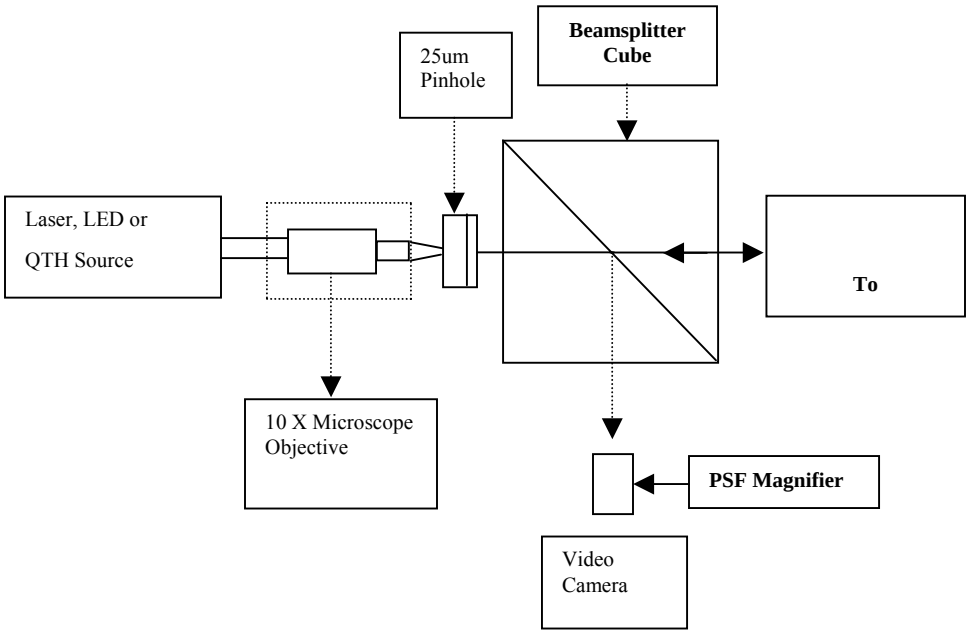

Fig #2

The source module is capable of supplying 633nm laser light (coarse alignments), white light from a QTH lamp or narrow band light from a series of high intensity LEDs (phasing operations).

10.2.2 SVIP SOURCE MODULE PHASE #2 (SYSTEM LEVEL TESTING):

The source module is modified for system level testing due to an impingement at the fold mirror used to feed light up to the detector bench. This optic blocks the line of sight between the source module and the BC secondary. To mitigate this problem, a fold flat and Pellicle beamsplitter were added to the receiver bench allowing light to pass through both benches.

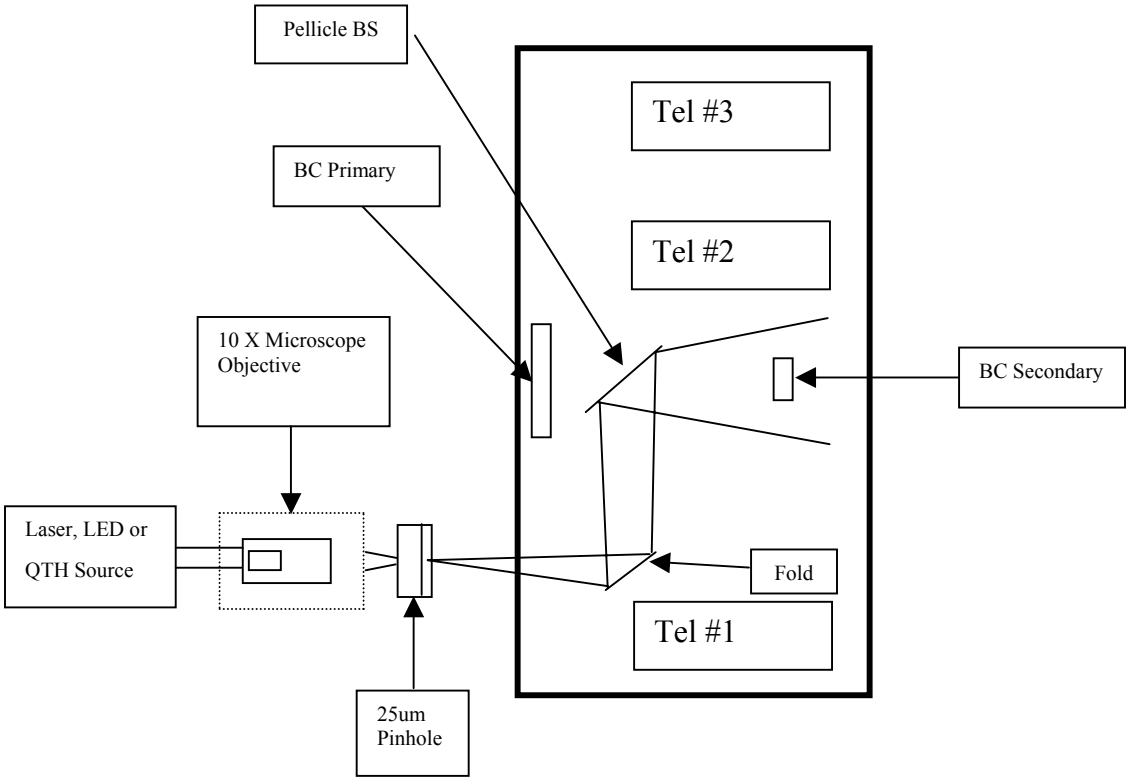

Fig #3

10.3 OVERVIEW OF PLAN FOR RECEIVER BENCH TESTING:

Following the initial alignment of the receiver bench (CMM and theodolites), the source module was aligned to the beam combiner secondary mirror. A Davidson autocollimator was used to verify collimation by viewing light reflected from the beam combiner primary.

Since we do not have access to a collimated source sufficiently large to simultaneously fill all three telescope apertures, the logical option was to inject light at the BC focus and propagate it through the system in double pass. Essentially, we pass light through the BC optics, BC folds, piston mechanisms, tip/tilt mirrors and then send it along the same path (nearly) after reflecting off a large flat mirror (or discrete folds) positioned before the telescopes.

At this time, three 6" diameter flat mirrors (on gimbal mounts) are acting as a surrogate for the large 53" X 4.5" X 3" test flat purchased for this application. Differential motions imparted between the discrete flats (channels (2-1) and (2-3)) allow controlled amounts of OPD to be introduced between telescope channels. This capability permits us to compensate for despace errors introduced during the optical alignment of the receiver bench (after the CMM work was completed). Each mirror was aligned in AZ (PAR) and EL (gravity) using theodolites and in despace using inside micrometers. The two outer retro-folds (telescopes 1 and 3) are mounted on motorized linear stages having a resolution of 0.1um.

These stages are used to balance path length variations between the reference scope (telescope #2) and channels 1 and 3. Angular changes imparted to components on the receiver bench (after the CMM alignment) could have potentially introduced despace errors on the order of millimeters. Without these stages, the path lengths would have to be balanced using the SVIP piston mechanisms (~38um travel) or by physically repositioning components on the bench.

Once the receiver bench has been phased, the path length corrections introduced (using the motorized stages) will be quantified and then compensated for using components on the receiver bench. Once this is completed, we would be in a position to convert over to the large flat in order to increase the temporal stability of the instrument when operating in a double pass configuration.

10.3.1 FIRST LIGHT, RECEIVER BENCH:

The source module (Phase #1) was aligned to the receiver bench in preparation for image assessment and phasing operations. Initial work was performed using a HeNE laser (spatially filtered) aligned on axis with the beam combiner secondary mirror. An autocollimator was used to position the source module in angle and to set the despace between the SM pinhole (25um) and the vertex of the BC secondary. Slight adjustments were made to the BC fold flat and telescope positions in order to pass light (single pass) through the bench without vignetting.

Next, the 6" return flats were positioned and aligned (in angle) before each of the three SVIP telescopes. We did not pay any particular attention to despace, since we did not plan to phase the system at this point in the alignment flow. A translucent screen defining the focal plane of the receiver bench was installed between the beamsplitting cube and video camera. With the video camera imaging the double passed returns from the three telescopes, the tip/tilt mechanisms were adjusted in order to superimpose the returns at nominal focus.

Once the imaging screen was removed it became evident that we had a problem. The image shown in below is typical of the double pass performance observed for each of the three SVIP telescopes. The image was collected from telescope #1 with the apertures of the remaining telescopes covered.

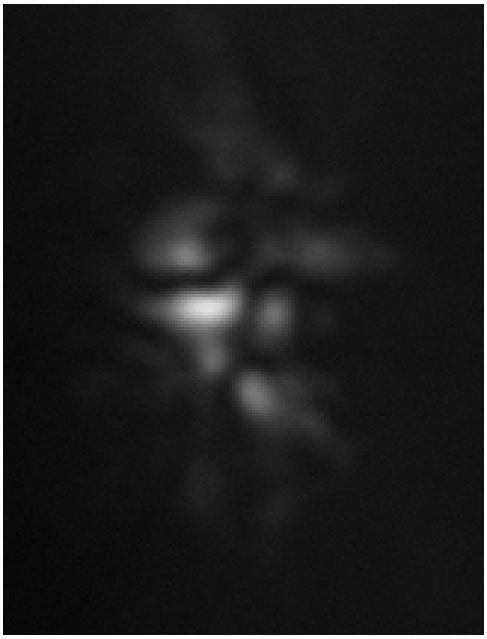

Fig. #4

Possible causes were thought to be one or more of the following:

- Alignment Errors (Not a good candidate due to the morphology)

- Vignetting At The Telescope Field Stop (or other optical component(s))
- Errors In The Beam combiner Optics
- Errors In the Primary and/or Secondary Mirrors

At the time this image was taken we were operating without the apertures installed at each of the tip/tilt mirrors. Adding these components helped (slightly) but did not significantly improve the imaging performance of the system.

We then adjusted the tip/tilt mirrors, thinking that we might be experiencing some diffraction effects at the edge of the field stops (telescope secondary mirrors). There was no evidence of vignetting, and no performance variation as a function of field point within the aperture. The output from the beam combiner was evaluated using an autocollimator and found to be acceptable.

With the 6" fold mirror removed from the front of telescope #1, the collimated beam exiting the telescope was viewed with a 5" Davidson autocollimator. Interestingly, this test showed some asymmetries in the PSF, but the small image scale prevented us from making a firm determination.

Telescope #1 was subsequently removed from the receiver bench and positioned before a ZYGO GPI interferometer. The interferometer was used as a source of collimated light to feed the PM of telescope #1. A fold mirror intercepted the collimated beam exiting the telescope secondary and delivered it to a camera after passing through a focusing lens. The resulting PSF showed significant amounts of energy outside of the core. This image is not indicative of the low order aberrations typically associated with alignment errors (*fig #5*).

Fig #5
Telescope #1, Single Pass, HeNe Source

We then re-measured the wavefront performance of the telescope and validated our original measurements of ~λ/20 RMS with a PV of ~0.28 waves. The results of this test are shown below (*fig. 6*).

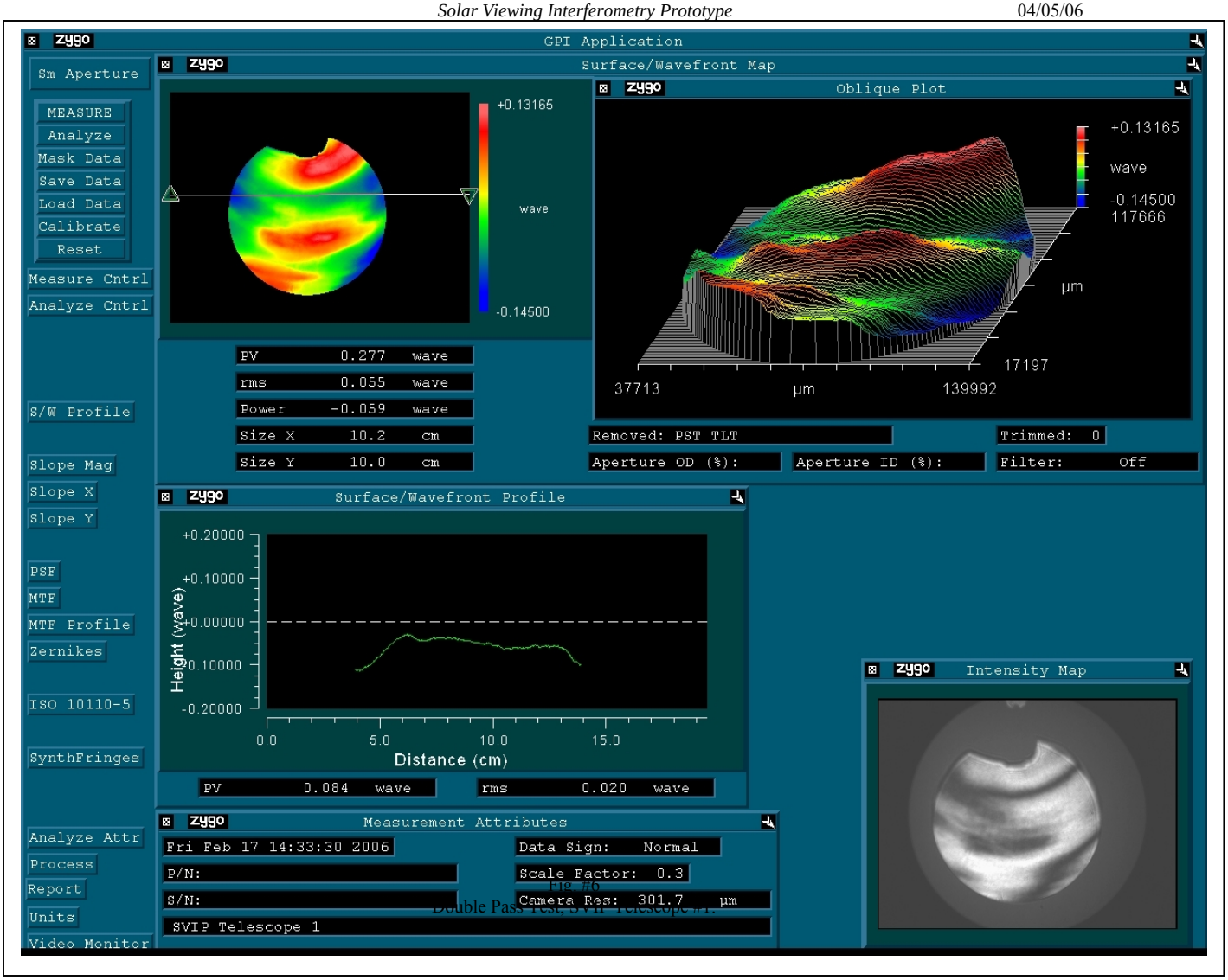

Fig. #5
Double Pass Test, SVIP Telescope #1.

The poor optical performance is the result of radial zones polished into both the primary and secondary mirrors during the manufacturing process. In retrospect, tighter control over the PV requirement would have prevented this condition from developing. Surprisingly, the Strehl ratio computed by the ZYGO interferometer was approximately 0.889. The "synthetic PSF" calculated using the ZYGO Metropro software did not indicate severity of the imaging problem though the zones are obviously visible in the fringe data. Fig. #7 shows the PSF and computed Strehl ratio for telescope #1 tested in double pass with an interferometric scale factor of 0.25.

Telescope #1, Synthetic PSF

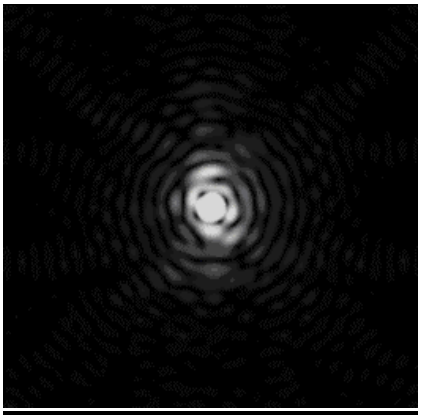

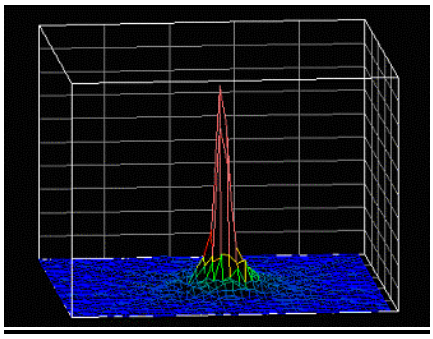

Fig 7

10.4 PREPARATION FOR PHASING THE RECEIVER BENCH

Though we had serious concerns over the performance of the three SVIP telescopes, we proceeded with our phasing plan. Initial work was performed using telescopes (2) and (3) since they had the smallest baseline separation. For this test, we used the configuration #1 source module described on page #2.

In preparation for phasing, we adjusted the tip/tilt mirrors and BC fold flats so that all three (double passed) images converged at the beam combiner focus (see fig #2). The trick here was to achieve this condition without eating up excessive amounts of the actuator dynamic range. The adjustments were made by making slight angular trades between the BC folds and the tip/tilt mirrors. It was quite difficult to introduce the controlled amounts of motion needed to achieve this condition. The situation was complicated by the fact that the actuators move beam along a 45 degree angle while to motions of the BC folds are pure AZ and EL (orthogonal). We never did achieve the goal of optically aligning all six channels with the corresponding PZT control voltages centered on the [0-10] volt range. Since we are nominally aligned and have sufficient travel to operationally correct the system (at least in a lab environment) we will declare success. As a field deployable system, this alignment would warrant further attention.

After completing the coarse alignments, the HeNe laser was removed from the source module and replaced with a liquid waveguide coupled to a 250 watt Oriel QTH lamp. The laser is useless in balancing the path lengths between channels due to its long coherence length.

10.4.1 PHASING, AND LIGHT THROUGHPUT PROBLEMS

Immediately after powering up the QTH lamp it was evident that we had a throughput problem. Even when running at maximum power (250 watts), we were still operating in a light starved environment. Since we are constrained to operate in double pass, we have work with the numerous disadvantages. From a throughput standpoint, we are not in good shape. We lose half of our initial light going through the beamsplitter followed by addition losses imparted by overfilling the BC secondary mirror. On the return path, we lose another factor of two going back through the beamsplitter cube. To make things worse, we have to double pass off of numerous reflecting surfaces on the receiver bench.

At these light levels, the use of an external Dispersed Fringe Sensor (DFS) would not be indicated. When we inserted a DFS (diffraction grating) into the converging between the beamsplitter cube and the video camera we saw nothing. Essentially, the use of a dispersive element decreased the flux at the focal plane to undetectable levels.

To improve throughput, we purchased several high power Light Emitting Diodes (LEDs) that were used to back illuminate the source module pinhole. These devices are extremely bright and provide the added benefit of being reasonably narrow band and incoherent. Though they were an improvement over the QTH lamp and fiber combination, the throughput was still insufficient to employ a DFS.

Without a DFS, the task of phasing the receiver bench is practically insurmountable. With possible path length differences approaching several millimeters[1] (between channels) it would be rather spectacular to stumble on the correct path to within a few hundred nanometers. We actually tried this approach and statistics won out.

10.5 CURRENT STATUS:

The detector bench has been mated with the receiver bench. A pellicle beamsplitter and fold mirror has been installed/aligned to the receiver bench as shown in Fig #3. With the system in this configuration we plan phase the receiver bench using the two DFS channels on the detector bench. The thought here is that we can adjust the camera integration time to counterbalance the low flux condition while improving the capture range from sub-microns to millimeters using the SVIP DFS.

[1] Several millimeters includes errors on bench and position errors with 6" return flats.

11.0 SUMMARY AND FUTURE WORK

SVIP is not currently operational because of problems associated with the surface characteristics of the primary mirrors for the telescopes. We believe that additional work, especially optically correcting the primary mirrors, would lead to an operational system.

Once this problem is corrected it should be possible to complete the alignment and test it with real or artificial sunlight as an input.

SVIP was an ambitious project involving new technology, new design work, and extensive mathematical analysis. The number of optical and mechanical parts exceeded 400, which is far beyond what was estimated when the project was proposed. The result is that the budget needed for completion was slightly underestimated by about 10%, and the time for completion was underestimated by about 25%. The budget shortfall was mostly caused by the switch to full-cost accounting. The tight budget with no margin is not unexpected for a project of this complexity that required almost 18 months of extensive optical and mechanical design. Our recommendation for such highly complex undertakings is that the development program not be locked rigidly into a fixed 3-year program and that there be some mechanism for additional funding based on a program review. In our case the situation was complicated by a proposal written before full cost accounting, which was not adjusted to compensate for the extra expenses of full cost accounting. The resulting budget shortfall required us to lower the specifications on the optical components from lambda/40 to lambda/20. We also experienced a 2-month funding delay followed by a 3-month budget lockout during the first year of the project that pushed us behind schedule. The 3-month delay was caused by Goddard switching to a new accounting system.

12.0 REFERENCES

[1] J.W. Hardy, Adaptive Optics for Astronomical Telescopes, Oxford University Press, 1998

13.0 APPENDICES

Optical

Doc 1 thru Doc 11